

Reactivity of a Stable Copper-Dioxygen Complex

Diana A. Iovan,^a Alexandra T. Wrobel,^a Arthur McClelland,^b Austin B. Scharf,^a Guy A. Edouard,^a and Theodore A. Betley^a

^a*Department of Chemistry and Chemical Biology, Harvard University, 12 Oxford Street, Cambridge, MA 02138*

^b*Center for Nanoscale Systems, Harvard University, 11 Oxford Street, Cambridge, MA 02138*

	Page
General Considerations.....	3
Characterization and Physical Measurements.....	3
Metal Complexes Syntheses.....	5
Reaction of (^A rL)Cu with Exogenous Ligands.....	9
Thermal Stability of (^A rL)Cu(O ₂).....	9
Reaction of (^A rL)Cu with Urea Hydroperoxide.....	10
Reactions of (^A rL)Cu(O ₂) with Substrates.....	10
Figure S1. Frozen toluene EPR spectrum of (^A rL)Cu(O–DMPO) (4).....	14
Figure S2. Frozen toluene EPR spectrum of (^A rL)CuCl (5).....	15
Figure S3. Frozen toluene EPR spectrum of (^A rL)Cu(OEt).....	16
Figure S4. Frozen toluene EPR spectrum of (^A rL)Cu(OPh).....	17
Figure S5. Frozen toluene EPR spectrum of (^A rL)Cu(O-p-C ₆ H ₄ OMe).....	18
Figure S6. Frozen toluene EPR spectrum of (^A rL)Cu(O(2-NH ₂ -4- ^t Bu-C ₆ H ₃)).....	19
Figure S7. ¹ H NMR spectra demonstrating ammonia binding to (^A rL)Cu.....	20
Figure S8. Orbitals obtained from a CAS(2,2) calculation using coordinates obtained from the truncated structure (^{Ph} L)Cu(O ₂) (2').....	21
Figure S9. ¹ H NMR spectra reveal reversible O ₂ binding.....	22
Figure S10. Variable temperature ¹ H NMR spectra of (^A rL)CuO ₂	23
Figure S11. UV-Vis spectrum of (^A rL)Cu(O ₂).....	24
Figure S12. Raman spectra of (^A rL)Cu(O ₂).....	25
Figure S13. Raman spectra comparison for (^A rL)Cu and (^A rL)Cu(O ₂).....	26
Figure S14. Frozen toluene EPR spectrum of complex 3 formed upon thermal decomposition of (^A rL)Cu(O ₂).....	27

Figure S15. Frozen toluene EPR spectrum of the reaction mixture of (^{Ar} L)Cu and urea hydroperoxide at 65 °C	28
Figure S16. Fit for the frozen toluene EPR spectrum of the reaction mixture of (^{Ar} L)Cu and urea hydroperoxide at 65 °C	29
Figure S17. Frozen toluene EPR spectrum of the reaction mixture of (^{Ar} L)Cu(O ₂) and 2-hydroxy-2-azaadamantane.....	30
Figure S18. Frozen toluene EPR spectrum of the reaction mixture of (^{Ar} L)Cu(O ₂) and 1,4-cyclohexadiene at 45 °C	31
Figure S19. Fit for the frozen toluene EPR spectrum of the reaction mixture of (^{Ar} L)Cu(O ₂) and 1,4-cyclohexadiene at 45 °C	32
Figure S20. Frozen toluene EPR spectra of the reaction mixtures of (^{Ar} L)Cu(O ₂) and phenols following HAA	33
Figure S21. Fit for frozen toluene EPR spectrum of the reaction mixture of (^{Ar} L)Cu(O ₂) and 2,4-di-tert-butylphenol (black).....	34
Figure S22. Fit for frozen toluene EPR spectrum of the reaction mixture of (^{Ar} L)Cu(O ₂) and 2,4,6-tri-tert-butylphenol (black)	35
Figure S23. Frozen toluene EPR spectrum of the reaction mixture of (^{Ar} L)Cu(O ₂) and phenol..	36
Figure S24. Frozen toluene EPR spectrum of the reaction mixture of (^{Ar} L)Cu(O ₂) and ammonium chloride	37
Figure S25. Iodometric detection of H ₂ O ₂ formation via UV-Vis.....	38
X-Ray Diffraction Techniques.....	39
Table S1. X-ray diffraction experimental details.....	41
Figure S26. Solid-state molecular structure for (^{Ar} L)Cu (1).....	42
Figure S27. Solid-state molecular structure for (^{Ar} L)Cu(O ₂) (2).....	43
Figure S28. Solid-state molecular structure for (^{Ar} L)Cu(O–DMPO) (4).....	44
Figure S29. Solid-state molecular structure for (^{Ar} L)CuCl (5).....	45
Figure S30. Solid-state molecular structure for (^{Ar} L)Cu(OEt) (6).....	46
Figure S31. Solid-state molecular structure for (^{Ar} L)Cu(OPh) (7).....	47
Computational Methods.....	48
Table S2. Percent contributions of the two singlet configurations to the ground state wavefunctions.	49
Table S3. Valence bond analysis of CAS(2,2) wavefunctions.	49
Table S4. XYZ Coordinates for (^{Ph} L)Cu(O ₂) (2') used for the CASSCF calculation.	49

General Considerations. All manipulations of metal complexes were carried out in the absence of water and dioxygen using standard Schlenk techniques or in an MBraun inert atmosphere drybox under a dinitrogen atmosphere. Ligand and ligand precursors were synthesized as previously reported.¹ All glassware was oven dried for a minimum of 1 h and cooled in an evacuated antechamber prior to use in the drybox. Benzene, diethyl ether, dichloromethane, n-hexane and tetrahydrofuran were dried over 4 Å molecular sieves (Strem) prior to use. Chloroform-*d* was purchased from Cambridge Isotope Labs and used as received. Benzene-*d*₆ was purchased from Cambridge Isotope Labs and was degassed and stored over 4 Å molecular sieves prior to use. Triphenylphosphine, 5,5-dimethyl-1-pyrroline-*N*-oxide, phenol, 4-methoxyphenol, 2,4-di-*tert*-butylphenol, 2,6-di-*tert*-butylphenol, 2,4,6-tri-*tert*-butylphenol, 2-amino-4-*tert*-butylphenol, ammonia (0.5 M in dioxane), 2-hydroxy-2-azaadamantane, thallium ethoxide, and ammonium chloride were purchased from Aldrich and used as received. Styrene, 1,4-cyclohexadiene, 1,3-cyclohexadiene, and dimethylsulfide were purchased from Aldrich and dried over molecular sieves prior to use. Celite® 545 (J. T. Baker) was dried in a Schlenk flask for 24 h under dynamic vacuum while heating to at least 150 °C prior to use in a drybox. Silica gel 32-63 μ (AIC, Framingham, MA) was used as received.

Characterization and Physical Measurements. ¹H and ¹³C NMR spectra were recorded on Varian Unity/Inova 400, 500 MHz- or Agilent DD2 600 MHz spectrometers. ¹H and ¹³C NMR chemical shifts are reported relative to SiMe₄ using the chemical shift of residual solvent peaks as reference. Gas chromatography/mass spectrometry (GC–MS) was performed on an Agilent GC–MS 5975 Turbo system using the following conditions: inlet temperature: 250 °C, oven temperature: 100 °C to 250 °C ramping over 10 min and holding for 8 min, solvent delay: 3 min. UV/Visible spectra were recorded on a Varian Cary 50 UV/Visible spectrometer using a quartz cuvette and a scan rate of 600 nm/ min. Elemental analyses were carried out on a Perkin Elmer 2400 Series II CHNS/O analyzer.

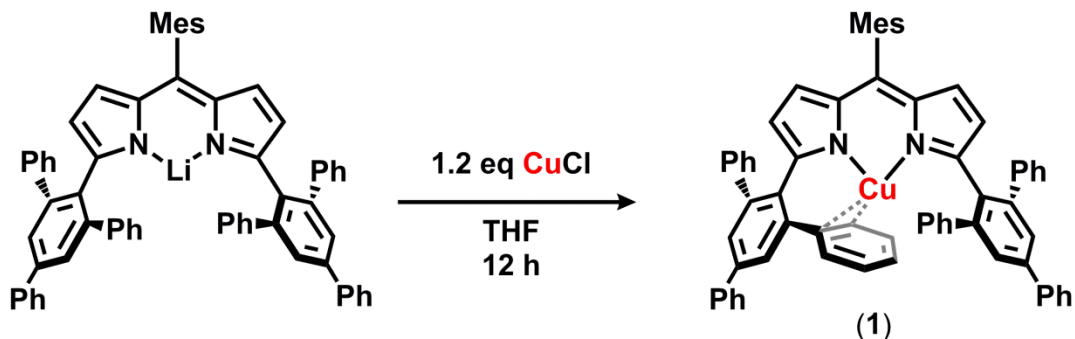
EPR spectra were obtained on a Bruker EleXsys E-500 CW-EPR spectrometer. Spectra were measured as frozen toluene glasses at a microwave power of 0.6325–2 mW. Spectral simulations were performed using EasySpin.²

¹ King, E. K.; Hennessy, E. T.; Betley, T. A. *J. Am. Chem. Soc.* **2011**, *133*, 8293.

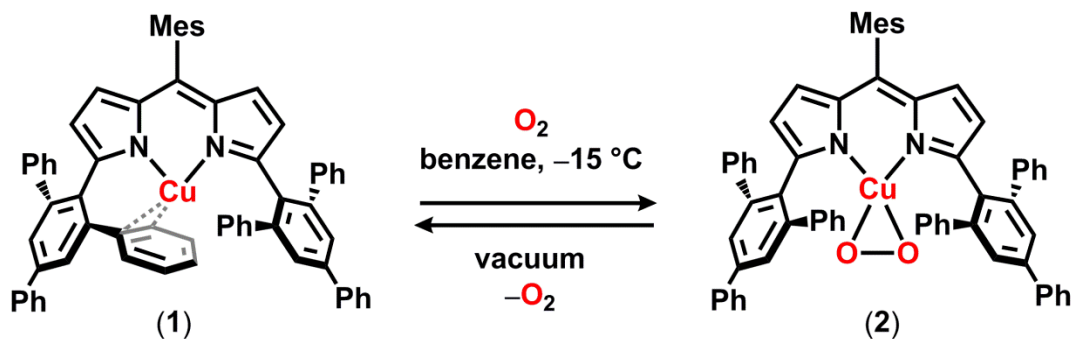
² Stoll, S.; Schweiger, A. *J. Magn. Reson.* **2006**, *178*, 42.

Raman measurements were collected at the Center for Nanoscale Systems (CNS) at Harvard University, a member of the National Nanotechnology Coordinated Infrastructure Network (NNCI). Raman spectra were recorded using a Horiba LabRam HR Evolution micro-Raman spectrometer featuring sub 1 cm^{-1} spectral resolution and sub- μm spatial resolution for confocal imaging. Measurements were performed using a 532 nm excitation laser, at room temperature. Samples were prepared in toluene and sealed in a J Young nmr tube. The $(^{\text{Ar}}\text{L})\text{Cu}(\text{O}_2)$ species was prepared through addition of stoichiometric dioxygen ($^{16}\text{O}_2$ or $^{18}\text{O}_2$) to a solution of $(^{\text{Ar}}\text{L})\text{Cu}$ (0.05 M) as described in the experimental section. The $(^{\text{Ar}}\text{L})\text{Cu}(\text{MeCN})$ was prepared via addition of acetonitrile to a solution of $(^{\text{Ar}}\text{L})\text{Cu}$ in toluene. $(^{\text{Ar}}\text{L})\text{Cu}(\text{MeCN})$ was prepared as a reference to account for potential vibrations arising due to the asymmetric ligand scaffold present in $(^{\text{Ar}}\text{L})\text{Cu}$, but not in $(^{\text{Ar}}\text{L})\text{Cu}(\text{O}_2)$.

Metal Complexes Syntheses

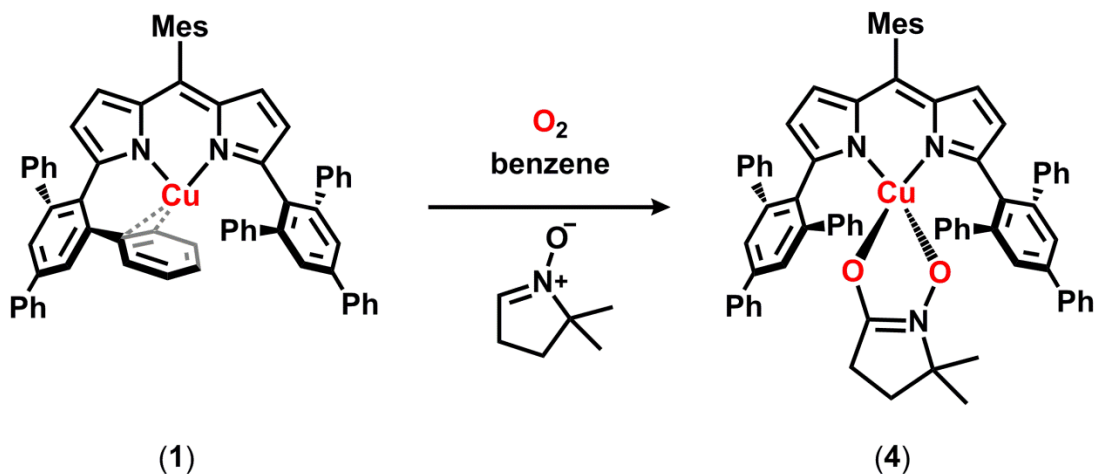


$(^{\text{Ar}}\text{L})\text{Cu}$ (1): Solid CuCl (120.2 mg, 1.21 mmol) was added to a solution of $(^{\text{Ar}}\text{L})\text{Li}$ (0.968 g, 1.104 mmol) in 20 mL of tetrahydrofuran and the mixture was allowed to stir at room temperature overnight. The reaction mixture was filtered through Celite and solvent was removed *in vacuo*. The resulting residue was collected in benzene, filtered through Celite, and the solvent lyophilized to afford $(^{\text{Ar}}\text{L})\text{Cu}$ as a purple powder. Recrystallization from a 2:1 mixture of hexanes and benzene at $-35\text{ }^{\circ}\text{C}$ afforded pure material (63 %) and crystals suitable for X-ray diffraction. $^1\text{H NMR}$ (500 MHz, C_6D_6) δ : 7.69 (s, 4H), 7.47–7.55 (m, 4H), 7.20–7.26 (m, 4H), 7.17 (d, $J = 7.32\text{ Hz}$, 2H), 7.10 (dd, $J = 8.08, 1.37\text{ Hz}$, 8H), 6.90–7.00 (m, 12H), 6.74 (s, 2H), 6.20 (d, $J = 3.97\text{ Hz}$, 2H), 5.86 (d, $J = 3.97\text{ Hz}$, 2H), 2.17 (s, 3H), 2.15 (s, 6H). $^{13}\text{C NMR}$ (125 MHz, C_6D_6) δ : 155.5, 145.1, 142.8, 140.7, 140.6, 140.5, 137.6, 136.8, 136.5, 136.4, 134.2, 129.1, 128.4, 128.3, 127.8, 127.8, 127.6, 127.4, 126.1, 125.2, 121.4, 21.1, 19.8. Anal. Calc. for $\text{C}_{66}\text{H}_{49}\text{CuN}_2$: C 84.90, H 5.29, N 3.00; Found: C 84.81, H 5.38, N 2.95.

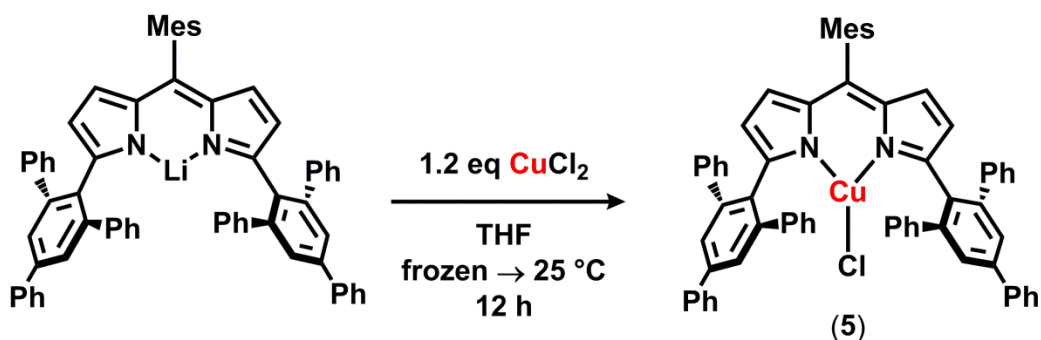


$(^{\text{Ar}}\text{L})\text{Cu}(\text{O}_2)$ (2): A solution of $(^{\text{Ar}}\text{L})\text{Cu}$ (1) in benzene was weighed into a 4 g scintillation vial, which was placed into a 20 g scintillation vial containing 10 mL of pentane. The vial was attached to a vacuum adaptor and the reaction mixture was sealed under nitrogen. The vial was

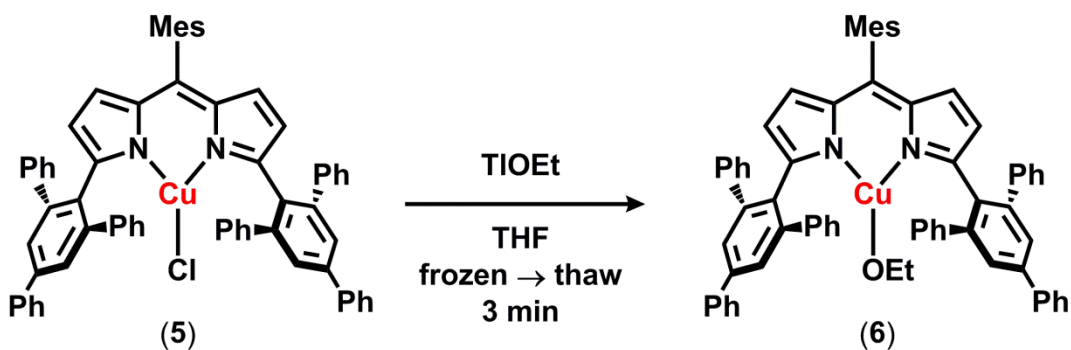
removed from the glovebox and connected to a Schlenk line. The reaction mixture was evacuated several times prior to addition of 1 atm of dioxygen. Upon warming to room temperature, a color change from purple to dark pink was noted. The reaction mixture was allowed to sit at room temperature for a day to allow for formation of crystals suitable for X-ray diffraction corresponding to $(^{Ar}L)Cu(O_2)$. 1H NMR (500 MHz, C_6D_6) δ : 7.97 (s, 4 H), 7.04–7.31 (m, 30 H), 6.70 (s, 2 H), 6.00 (d, $J = 3.81$ Hz, 2 H), 5.82 (d, $J = 4.58$ Hz, 1 H), 2.18 (s, 3 H), 1.87 (s, 6 H). ^{13}C NMR (125 MHz, C_6D_6) δ : 160.9, 142.5, 142.8, 141.0, 137.4, 136.6, 136.2, 135.6, 134.0, 132.7, 130.4, 130.0, 129.0, 128.7, 128.5, 126.7, 123.2, 21.1, 19.52.



$(^{Ar}L)Cu(O-DMPO)$ (4): A solution of $(^{Ar}L)Cu$ (1) and 5,5-dimethyl-1-pyrroline-*N*-oxide (1 equiv) in benzene was transferred to a pressure vessel and removed from the glovebox. Note: no reaction occurs between 1 and DMPO. The flask was evacuated and a slight excess of dioxygen was added to the frozen reaction mixture, filling up to 1 atm with dinitrogen. The reaction was allowed to warm to room temperature and proceed for 24 h. The flask was evacuated to remove any excess dioxygen and was brought back into the glovebox. The solvent was removed *in vacuo* to afford a purple-pink powder. Crystals suitable for X-ray diffraction confirming formation of $(^{Ar}L)Cu(O-DMPO)$ were obtained from a solution of hexanes with minimal benzene containing the isolated powder. 1H NMR (500 MHz, C_6D_6) δ : 8.54 (br. s), 7.94 (br. s), 7.39 (s), 7.10 (s), 6.52 (s), 1.95 (s), -1.03 , -4.95 .

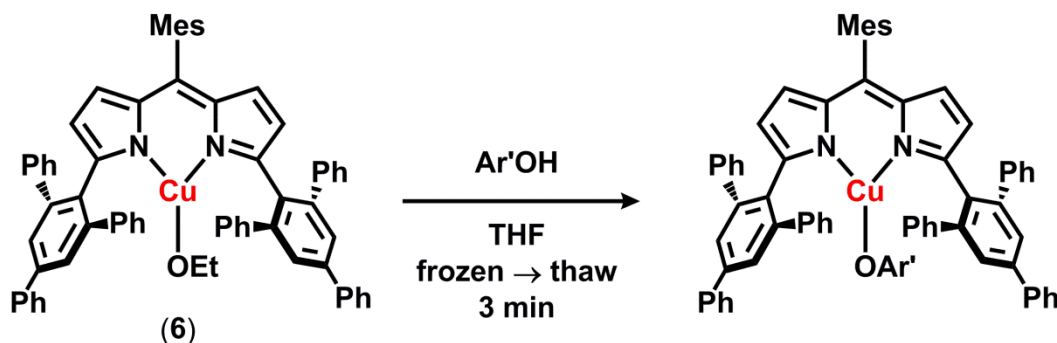


(^{Ar}L)CuCl (5): A thawing tetrahydrofuran (5 mL) solution of (^{Ar}L)Li (148.9 mg, 0.17 mmol) was added to a frozen solution of CuCl₂ (27.6 mg, 0.205 mmol) in 1 mL of tetrahydrofuran and the mixture was allowed to warm to room temperature and stir overnight. The reaction mixture was filtered through Celite and solvent was removed *in vacuo*. The resulting residue was collected in benzene, filtered through Celite, and the solvent lyophilized to afford (^{Ar}L)CuCl as a pink-purple powder (97%). Crystals suitable for X-ray diffraction were obtained from a saturated hexanes solution at $-35\text{ }^{\circ}\text{C}$. ¹H NMR (400 MHz, C₆D₆): δ 8.91 (br. s), 7.99 (br. s), 7.01 (s), 6.81 (s), 6.55 (br. s), 1.93 (s). Anal. Calc. for C₆₆H₄₉ClCuN₂: C 81.80, H 5.10, N 2.89; Found: C 81.68, H 4.99, N 2.83.



(^{Ar}L)Cu(OEt) (6): A thawing solution of (^{Ar}L)CuCl (5) (82.9 mg, 0.0855 mmol) in 5 mL of tetrahydrofuran was added to a frozen solution of thallium ethoxide (22 mg, 0.0882 mmol) in 0.5 mL of tetrahydrofuran and the reaction was allowed to thaw and stir cold for 3 minutes and solvent was removed *in vacuo* immediately afterwards. The resulting residue was collected in hexanes, filtered through Celite to remove thallium chloride, and concentrated *in vacuo*. The resulting residue was then dissolved in benzene and solvent lyophilized to afford a dark purple-pink powder (83%). Crystals suitable for X-ray diffraction were obtained from diffusing pentane into a saturated tetrahydrofuran solution of (^{Ar}L)Cu(OEt) at $-35\text{ }^{\circ}\text{C}$. ¹H NMR (400 MHz,

C_6D_6) δ : 8.75 (br. s), 8.15 (br. s), 6.95 (s), 6.54 (br. s), 1.91 (s), -5.75 (br. s). Anal. Calc. for $C_{68}H_{54}CuN_2O$: C 83.45, H 5.56, N 2.86; Found: C 83.46, H 5.55, N 3.02.



$OAr' = OPh$ (7), $O-p-C_6H_4OMe$ (8),
 $O(2-NH_2-4-tBu-C_6H_3)$ (9)

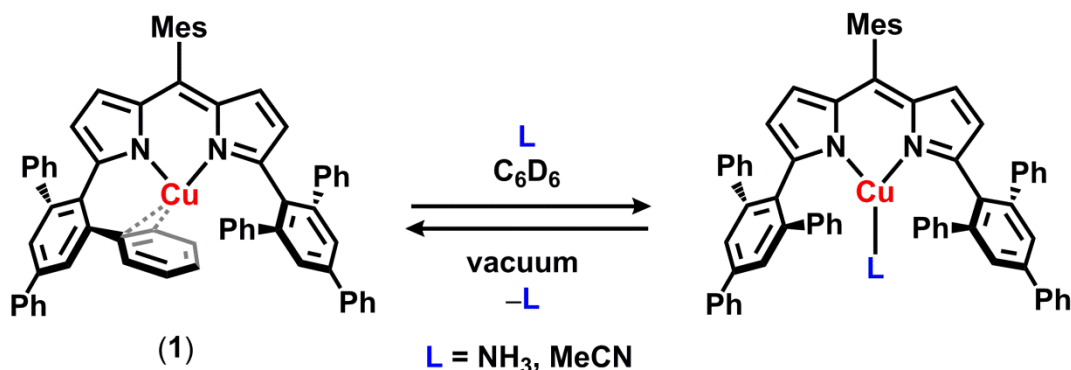
General procedure for synthesis of $(ArL)Cu(OAr')$: A solution of the corresponding phenol (1 equiv) in tetrahydrofuran was added to a thawing solution of $(ArL)Cu(OEt)$ (6) (1 equiv) in 5 mL of tetrahydrofuran. The resulting mixture was stirred at room temperature for 5 minutes and solvent was then removed *in vacuo*. The residue was triturated with hexanes twice to remove the ethanol byproduct. The resulting solid was collected in benzene and lyophilized to afford $(ArL)Cu(OAr')$ as a pink-purple powder.

$(ArL)Cu(OPh)$ (7): 18.4 mg, 87%. 1H NMR (500 MHz, C_6D_6) δ : 8.81 (br. s), 8.21 (br. s), 6.95 (s), 6.56 (s), 6.17 (br. s), 1.95 (s). Anal. Calc. for $C_{72}H_{54}CuN_2O$: C 84.22, H 5.30, N 2.73; Found: C 84.14, H 5.25, N 3.07.

$(ArL)Cu(O-p-C_6H_4OMe)$ (8): 1H NMR (500 MHz, C_6D_6) δ : 18.31 (br. s), 8.66 (br. s), 8.15 (s), 6.65 (s), 6.47 (s), 1.98 (s). Note: the reaction with 4-methoxyphenol does not proceed cleanly even at low temperatures, reduction to **1** is always observed in addition to the desired product. As such, elemental analysis was not acquired on this complex.

$(ArL)Cu(O(2-NH_2-4-tBu-C_6H_3))$ (9): 16.9 mg, 90%. 1H NMR (500 MHz, C_6D_6) δ : 21.25 (s), 10.08 (br. s), 9.51 (s), 9.05 (s), 8.51 (s), 6.46 (m), 6.34 (m), 5.78 (m), 5.58 (br. s), 5.48 (m), 5.17 (s), 4.21 (s), 3.38 (s), -6.77 (s), -12.91 (s), -18.25 (br. s). Anal. Calc. for $C_{76}H_{63}CuN_3O$: C 83.14, H 5.78, N 3.83; Found: C 83.01, H 5.62, N 4.18.

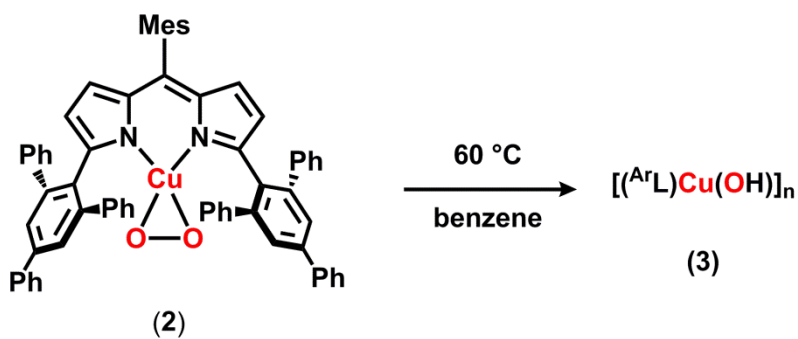
Reaction of (^{Ar}L)Cu with Exogenous Ligands



Under an inert N₂ atmosphere, acetonitrile or a solution of ammonia (0.5 M in dioxane) was added to a solution of (^{Ar}L)Cu (**1**) in benzene-*d*₆ to observe an immediate color change from purple to intense pink. ¹H NMR analysis revealed conversion to a symmetric three-coordinate solvento-adduct (^{Ar}L)Cu(L) (L = MeCN or NH₃). Upon removal of solvent *in vacuo*, a color change to purple was noticed and regeneration of **1** was confirmed via ¹H NMR (Fig. S7).

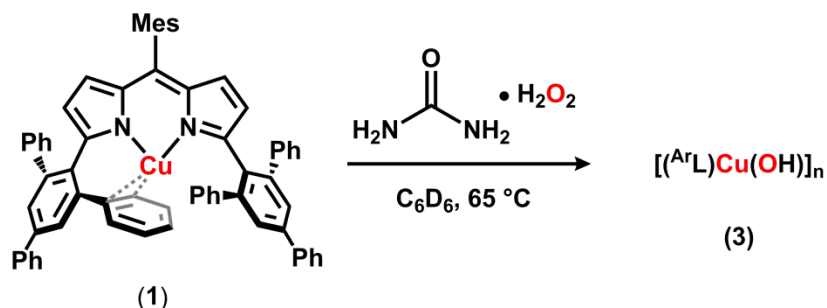
Thermal Stability of (^{Ar}L)Cu(O₂)

Under an inert N₂ atmosphere, a solution of (^{Ar}L)Cu (**1**) in benzene-*d*₆ was transferred to a J Young NMR tube. The solution was evacuated and exposed to slight excess of dioxygen, filling up to 1 atm with dinitrogen. The (^{Ar}L)Cu(O₂) (**2**) generated *in situ* was tracked via ¹H NMR, displaying no decay over the course of days at room temperature. No decomposition was visible upon mild heating to 45 °C, however, heating the solution above 50 °C results in slow conversion to an intense purple Cu^{II} species (**3**). Upon full consumption of (^{Ar}L)Cu(O₂) (**2**), the solution was evacuated to remove unreacted dioxygen and was brought back into the glovebox to remove the solvent *in situ*. The resultant material was analyzed via EPR (Fig. S12).



Reaction of (^{Ar}L)Cu with Urea Hydroperoxide

Under an inert N₂ atmosphere, solutions of (^{Ar}L)Cu (**1**) and urea hydroperoxide in benzene-*d*₆ were transferred to a J Young NMR tube. The reaction mixture was heated to 65 °C for 24 h to afford an intense dark purple solution. Upon cooling to room temperature, the solution was filtered and the solvent removed *in vacuo* to afford a dark purple solid (**3**) which was analyzed by ¹H NMR and EPR (Fig. S13).



Reactions of (^{Ar}L)Cu(O₂) with Substrates

Reactions with hydrogen atom sources

Under an inert N₂ atmosphere, solutions of (^{Ar}L)Cu (**1**) and either 1,4-cyclohexadiene or 2-hydroxy-2-azaadamantane in benzene-*d*₆ were transferred to a J Young NMR tube. ¹H NMR analysis revealed no change to the copper species upon addition of substrate. The resultant solution was evacuated and exposed to slight excess of dioxygen, filling up to 1 atm with dinitrogen. Reactions were monitored by ¹H NMR, tracking consumption of the (^{Ar}L)Cu(O₂) (**2**). The reaction with 1,4-cyclohexadiene was heated to 45 °C, whereas the reaction with 2-hydroxy-2-azaadamantane proceeds at room temperature. Upon full consumption of (^{Ar}L)Cu(O₂) (**2**), the solutions were evacuated to remove any unreacted dioxygen and were brought back into the glovebox to remove the solvent *in vacuo*. The resulting materials were analyzed via EPR (Fig. S14 and S15).

Reaction of **2** with 2-hydroxy-2-azaadamantane results in rapid generation of the corresponding *N*-oxide radical as corroborated by EPR (the spectrum matches that of authentic 2-azaadamantane-*N*-oxyl (Fig. S14).

Reaction of **2** with 1,4-cyclohexadiene afforded a not well-defined EPR spectrum, but with features similar to that of **3** (Fig. S15 and S16), suggesting that HAA is likely taking place.

However, in the absence of identification of either the organic product or the copper-containing species, alternate reaction pathways cannot be excluded (e.g., insertion into the C–H bond or reaction with the olefin moiety). Attempts to monitor the reaction of **2** with fluorene instead (similar BDE for the C–H bond) resulted in no reaction after heating to 50 °C (higher temperatures would promote thermal decay of **2** as described above), likely due to steric constraints.

Reactions with phenol substrates

Under an inert N₂ atmosphere, solutions of (^{Ar}L)Cu (**1**) and the appropriate phenol in benzene-*d*₆ were transferred to a J Young NMR tube. ¹H NMR analysis revealed no change to the copper species upon addition of substrate. The resultant solution was evacuated and exposed to slight excess of dioxygen, filling up to 1 atm with dinitrogen. Reactions were monitored by ¹H NMR, tracking consumption of the (^{Ar}L)Cu(O₂) (**2**). Reactions with phenol, 4-nitrophenol, 2-amino-4-*tert*-butylphenol, and 4-methoxyphenol proceeded at room temperature. Reactions with 2,6-di-*tert*-butylphenol, 2,4-di-*tert*-butylphenol, or 2,4,6-tri-*tert*-butylphenol were heated to 45 °C. Upon full consumption of (^{Ar}L)Cu(O₂) (**2**) or substrate, the solutions were evacuated to remove any unreacted dioxygen and were brought back into the glovebox to remove the solvent *in vacuo*. The resulting materials were analyzed via EPR, GC–MS, and ¹H NMR (Fig. S17 and S20). The reaction with 2,4,6-tri-*tert*-butylphenol did not fully consume **2**, but all the phenol substrate was consumed after heating to 45 °C for several hours.

All reactions with acidic phenols (acid-base chemistry) proceeded fast and consumed all substrate to afford the corresponding copper phenoxide complexes and an additional unidentified copper-containing species as confirmed via both EPR and ¹H NMR. The reaction with 2,4-di-*tert*-butylphenol proceeded at 45 °C to afford the C–C coupled product quantitatively (> 98%) as confirmed via GC–MS and ¹H NMR (no other organic product was detected, minor amount of unreacted phenol noted by GC–MS). The reactions with 2,4,6-tri-*tert*-butylphenol afforded the corresponding 2,6-di-*tert*-butyl-1,4-benzoquinone quantitatively (> 98%) as confirmed via GC–MS (no other major organic products could be detected via either GC–MS or ¹H NMR). The reaction with 2,6-di-*tert*-butylphenol afforded the corresponding 2,6-di-*tert*-butyl-1,4-benzoquinone, albeit some unreacted phenol was observed via GC–MS.

Iodometric detection of hydrogen peroxide³

The reaction of **2** with phenol was set up in a Schlenk flask in a similar manner as described above. After 24 h, the reaction mixture was opened to air and quenched with 3 equiv of HCl. A small amount of that mixture was then transferred to a saturated solution of sodium iodide in acetonitrile. After approximately 30 min, the UV-Vis spectrum was collected and I_3^- was identified at $\lambda = 362$ nm (Fig. S22).

Reactions with ammonium chloride

Under an inert N_2 atmosphere, solutions of (^{Ar}L)Cu (**1**) and ammonium chloride in tetrahydrofuran were transferred to a J Young NMR tube. 1H NMR analysis revealed no change to the copper species upon addition of substrate. The resultant solution was evacuated and exposed to slight excess of dioxygen, filling up to 1 atm with dinitrogen. The reaction was allowed to proceed at room temperature and monitored by 1H NMR, tracking consumption of the (^{Ar}L)Cu(O₂) (**2**). Upon full consumption of (^{Ar}L)Cu(O₂) (**2**) or substrate, the solutions were evacuated to remove any unreacted dioxygen and were brought back into the glovebox to remove the solvent *in vacuo*. The resulting materials were analyzed via EPR and 1H NMR (Fig. S21).

Reaction with triphenylphosphine

A: Under an inert N_2 atmosphere, solutions of (^{Ar}L)Cu (**1**) and triphenylphosphine in benzene-*d*₆ were transferred to a J Young NMR tube. 1H NMR analysis revealed triphenylphosphine binding to **1**. The resultant solution was evacuated and exposed to slight excess of dioxygen, filling up to 1 atm with dinitrogen. The reaction was allowed to proceed at room temperature and was monitored by 1H NMR, tracking consumption of the (^{Ar}L)Cu(O₂) (**2**). Upon full consumption of (^{Ar}L)Cu(O₂) (**2**), the solution was evacuated to remove any unreacted dioxygen and was brought back into the glovebox to remove the solvent *in vacuo*. The resulting material was analyzed via EPR, GC-MS, and ^{31}P NMR to reveal quantitative formation of triphenylphosphine oxide.

B: Under an inert N_2 atmosphere, a solution of (^{Ar}L)Cu (**1**) in benzene-*d*₆ was transferred to an NMR tube sealed with a septum. The solution was evacuated and exposed to slight excess of dioxygen, filling up to 1 atm with dinitrogen. A solution of triphenylphosphine in benzene-*d*₆ (prepared under an inert N_2 atmosphere) was then added through a syringe. The reaction was

³ Procedure similar to: Tano, T.; Okubo, Y.; Kunishita, A.; Kubo, M.; Sugimoto, H.; Fujieda, N.; Ogura, T.; Itoh, S. *Inorg. Chem.* **2013**, *52*, 10431.

allowed to proceed at room temperature and was monitored by ^1H NMR. Immediate consumption of ($^{\text{A}}\text{L}$)Cu(O₂) (**2**) was noted. The resulting material was analyzed via GC–MS and ^{31}P NMR to reveal quantitative formation of triphenylphosphine oxide.

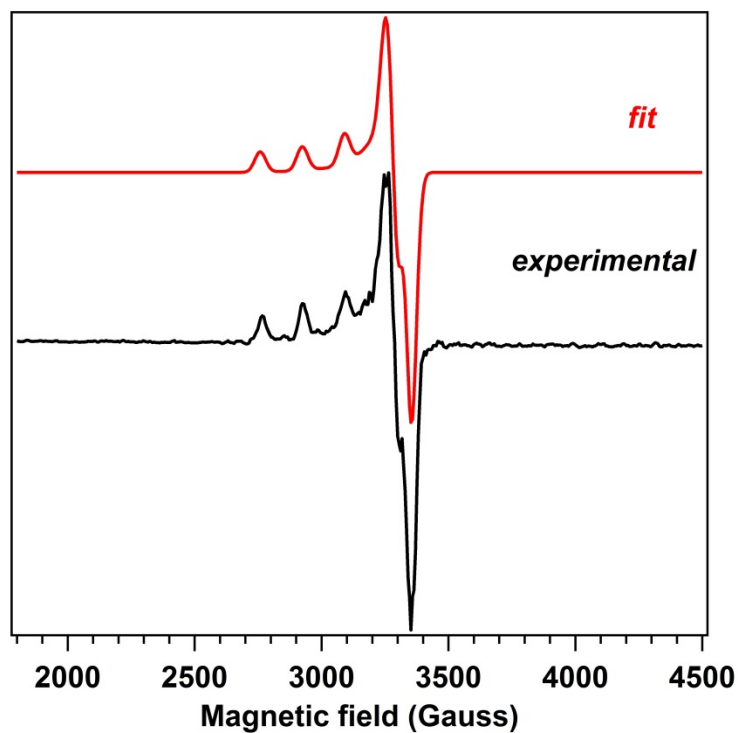


Figure S1. Frozen toluene EPR spectrum of (^{Ar}L)Cu(O-DMPO) (**4**) at 77 K expanded to show the rhombic signal (black), 9.449049 GHz. The red line represents a fit with Easyspin² for an $S = 1/2$ spin state, with the following parameters: $g_1 = 2.24$, $g_2 = 2.048$, $g_3 = 2.057$, $A_1 = 520$ MHz, $A_2 = 9.77$ MHz, $A_3 = 38.5$ MHz, linewidth = 4.30 mT.

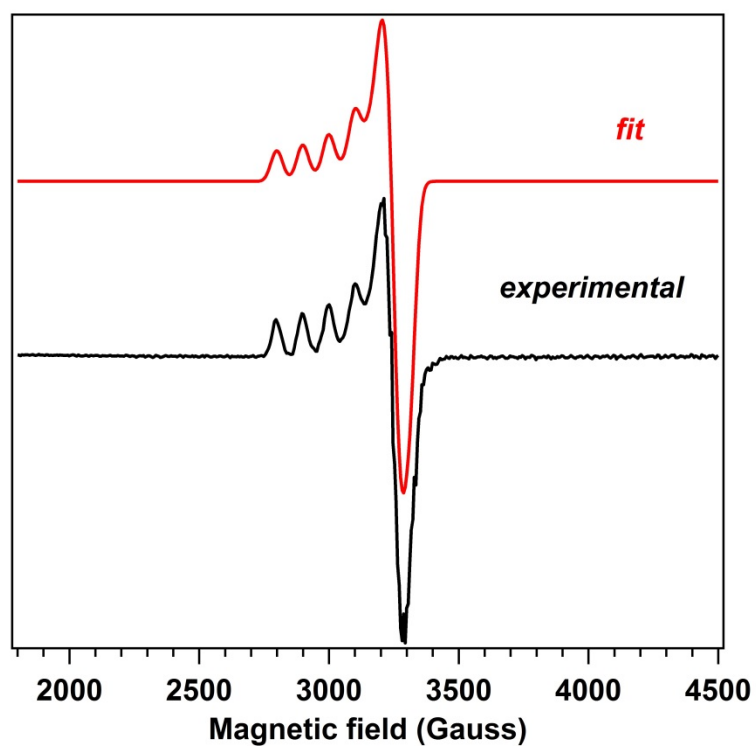


Figure S2. Frozen toluene EPR spectrum of (^{Ar}L)CuCl (**5**) at 77 K expanded to show the rhombic signal (black), 9.448259 GHz. The red line represents a fit with Easyspin² for an $S = 1/2$ spin state, with the following parameters: $g_1 = 2.29$, $g_2 = 2.087$, $g_3 = 2.052$, $A_1 = 320$ MHz, $A_2 = 34.8$ MHz, $A_3 = 53.9$ MHz, linewidth = 4.45 mT.

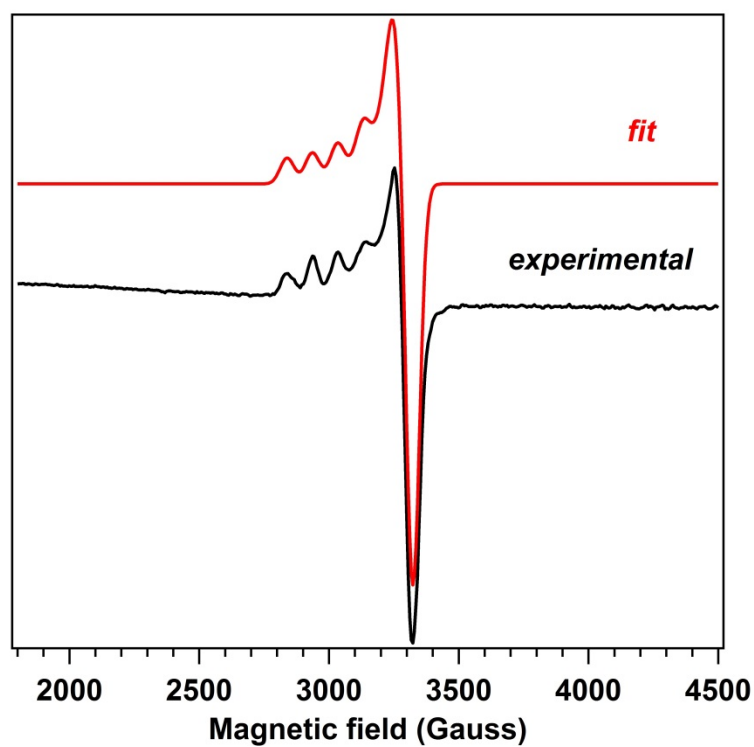


Figure S3. Frozen toluene EPR spectrum of (^{Ar}L)Cu(OEt) (**6**) at 77 K expanded to show the rhombic signal (black), 9.453164 GHz. The red line represents a fit with Easyspin² for an $S = 1/2$ spin state, with the following parameters: $g_1 = 2.26$, $g_2 = 2.04$, $g_3 = 2.057$, $A_1 = 301$ MHz, $A_2 = 19.8$ MHz, $A_3 = 42.9$ MHz, linewidth = 5.4 mT.

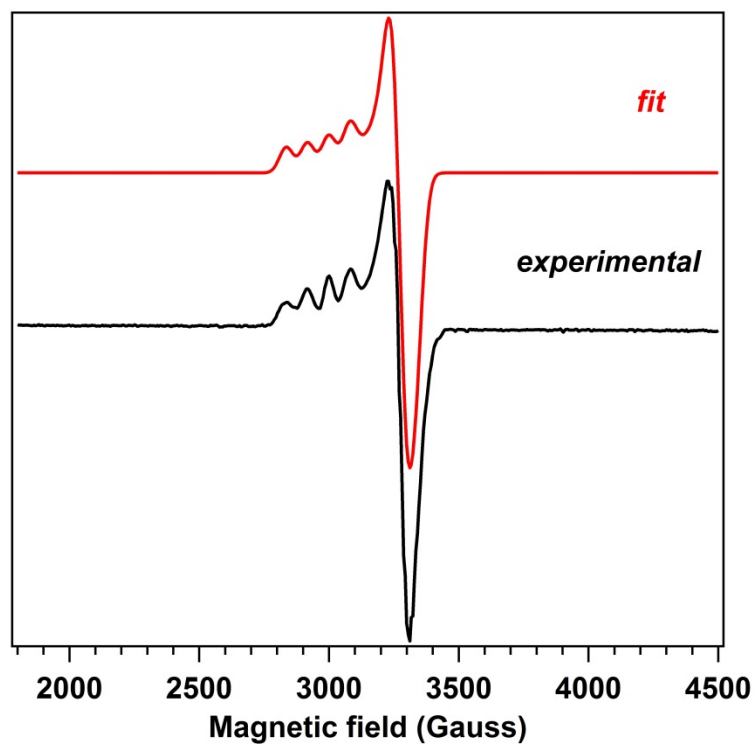


Figure S4. Frozen toluene EPR spectrum of (^{Ar}L)Cu(OPh) (**7**) at 77 K expanded to show the rhombic signal (black), 9.445994 GHz. The red line represents a fit with Easyspin² for an $S = 1/2$ spin state, with the following parameters: $g_1 = 2.28$, $g_2 = 2.065$, $g_3 = 2.035$, $A_1 = 260$ MHz, $A_2 = 29.8$ MHz, $A_3 = 57.5$ MHz, linewidth = 5.21 mT.

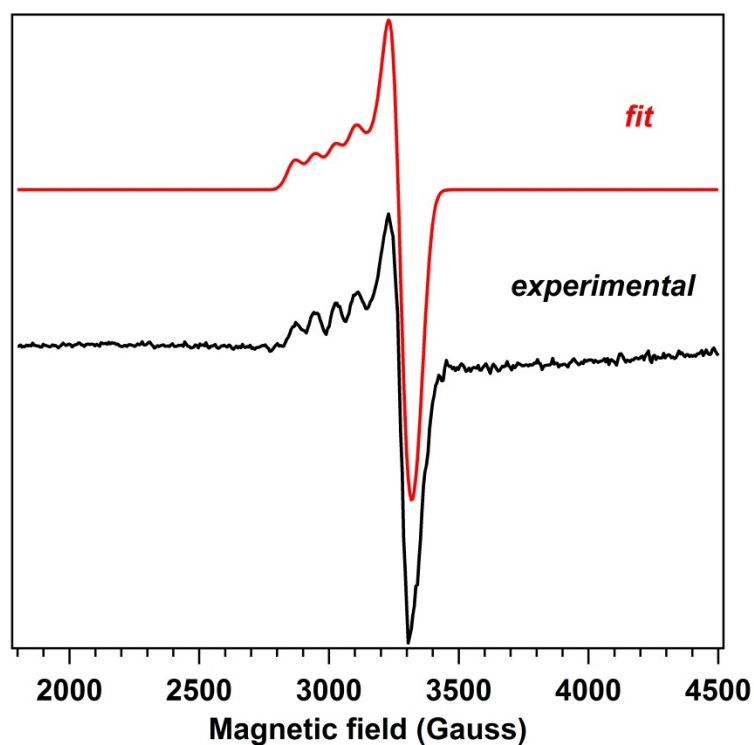


Figure S5. Frozen toluene EPR spectrum of (^{Ar}L)Cu(O-*p*-C₆H₄OMe) (**8**) at 77 K expanded to show the rhombic signal (black), 9.447048 GHz. The red line represents a fit with Easyspin² for an $S = 1/2$ spin state, with the following parameters: $g_1 = 2.26$, $g_2 = 2.067$, $g_3 = 2.027$, $A_1 = 245$ MHz, $A_2 = 14.8$ MHz, $A_3 = 47.8$ MHz, linewidth = 5.805 mT.

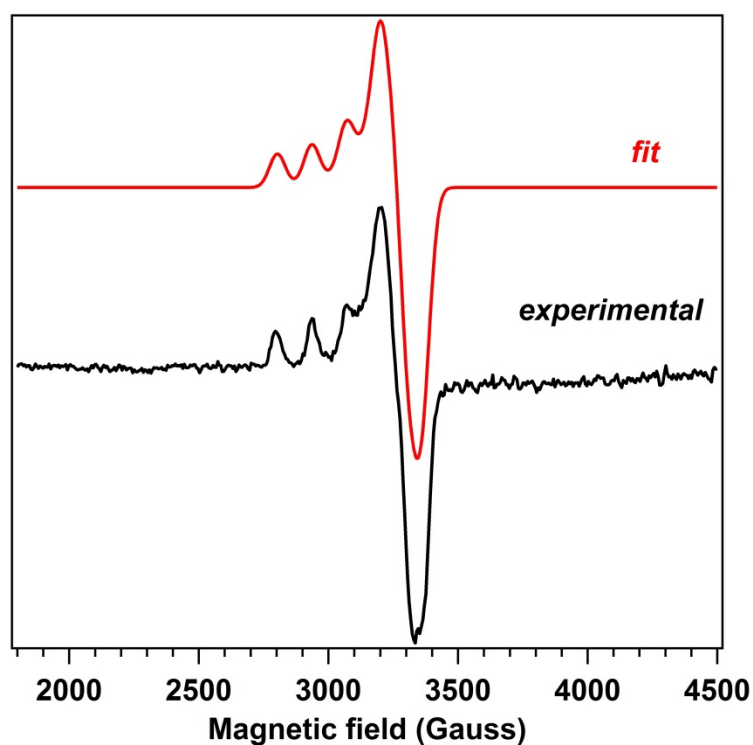
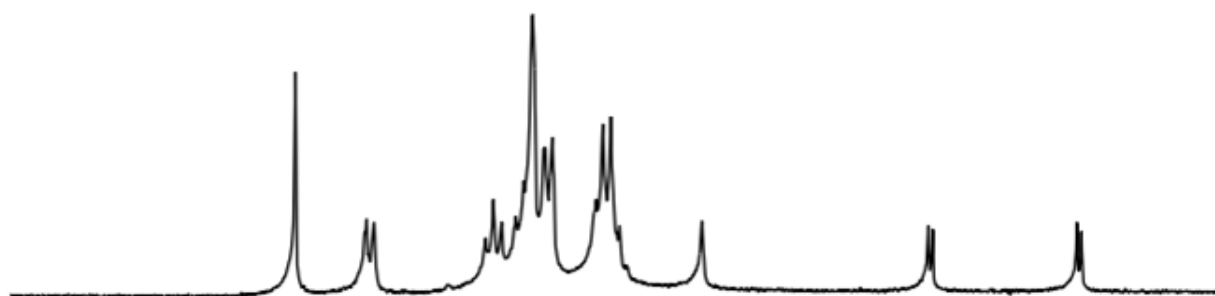


Figure S6. Frozen toluene EPR spectrum of (^{Ar}L)Cu(O(2-NH₂-4'-Bu-C₆H₃)) (**9**) at 77 K expanded to show the rhombic signal (black), 9.447962 GHz. The red line represents a fit with Easyspin² for an $S = 1/2$ spin state, with the following parameters: $g_1 = 2.25$, $g_2 = 2.021$, $g_3 = 2.088$, $A_1 = 417$ MHz, $A_2 = 24.8$ MHz, $A_3 = 53.9$ MHz, linewidth = 6.047 mT.

$(^{\text{Ar}}\text{L})\text{Cu}$ (**1**)



$(^{\text{Ar}}\text{L})\text{Cu}(\text{NH}_3)$

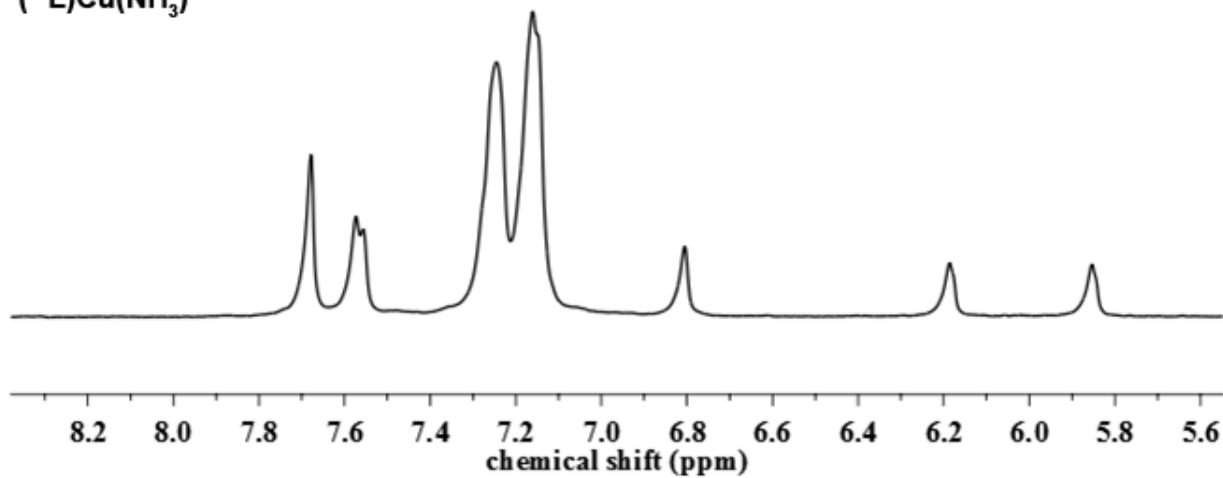


Figure S7. ¹H NMR spectra demonstrating ammonia binding to $(^{\text{Ar}}\text{L})\text{Cu}$: (top) $(^{\text{Ar}}\text{L})\text{Cu}$ (**1**); (bottom) spectrum of $(^{\text{Ar}}\text{L})\text{Cu}(\text{NH}_3)$ generated upon addition of a solution of ammonia in dioxane to **1** in benzene-*d*₆.

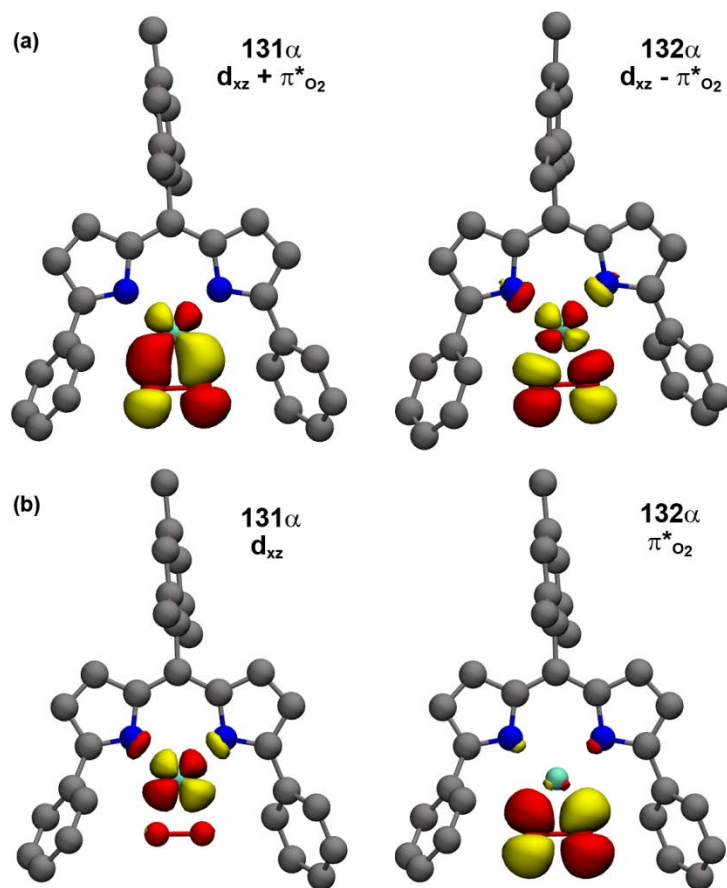


Figure S8. Orbitals obtained from a CAS(2,2) calculation using coordinates obtained from the truncated structure $(\text{PhL})\text{Cu}(\text{O}_2)$ ($2'$): (a) the two orbitals in the active space 131α ($d_{xz} + \pi^*_{\text{O}_2}$) – occupation 1.653589 and 132α ($d_{xz} - \pi^*_{\text{O}_2}$) – occupation 0.346411; (b) localized molecular orbitals 131α (d_{xz}) – 96.3742% Cu and 132α ($\pi^*_{\text{O}_2}$) – 51.4631% and 42.3428% for the two O atoms, respectively.

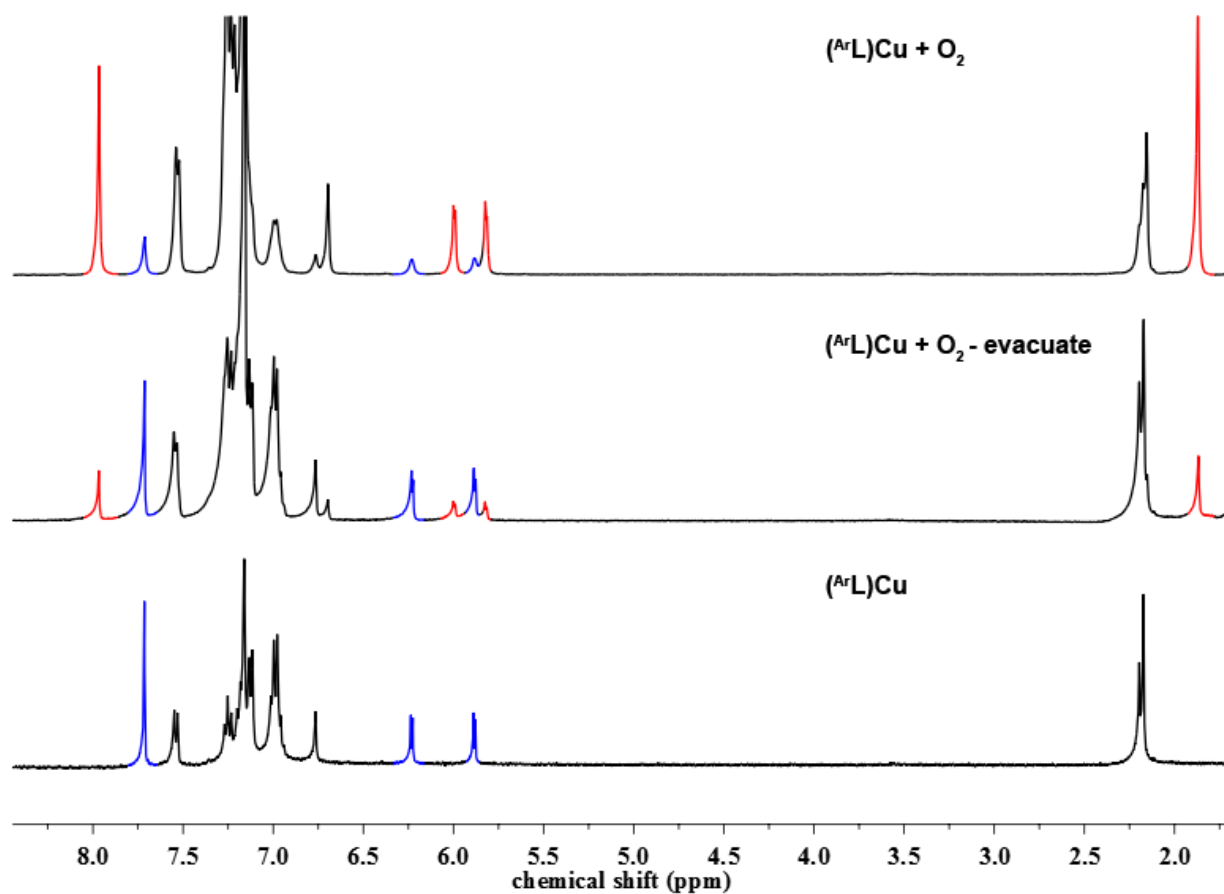


Figure S9. ^1H NMR spectra reveal reversible O_2 binding to $(^{\text{Ar}}\text{L})\text{Cu}$ upon vacuum exposure: **(top)** spectrum upon addition of 1 eq O_2 to $(^{\text{Ar}}\text{L})\text{Cu}$ (**1**); **(middle)** spectrum after one evacuation cycle showing a decrease in amount of **2**; **(bottom)** authentic spectrum of **1**. Representative signals for **1** and **2** are highlighted in blue (**1**) and red (**2**), respectively.

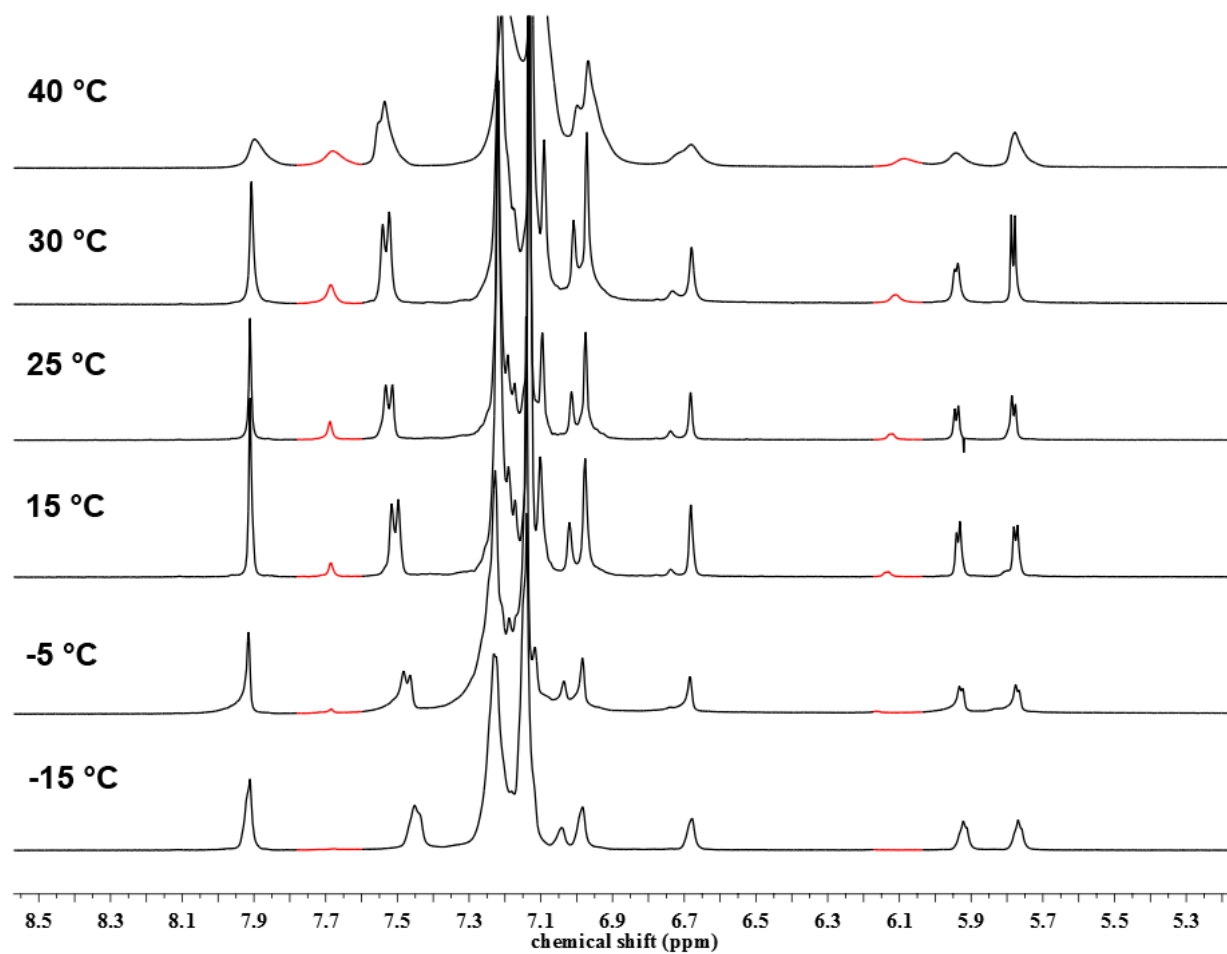


Figure S10. Variable temperature ^1H NMR spectra of $(\text{ArL})\text{CuO}_2$ reveals reversible O_2 binding to $(\text{ArL})\text{Cu}$. Representative signals for $(\text{ArL})\text{Cu}$ are highlighted in red to show that as the solution mixture is cooled, equilibrium shifts to $(\text{ArL})\text{Cu}(\text{O}_2)$.

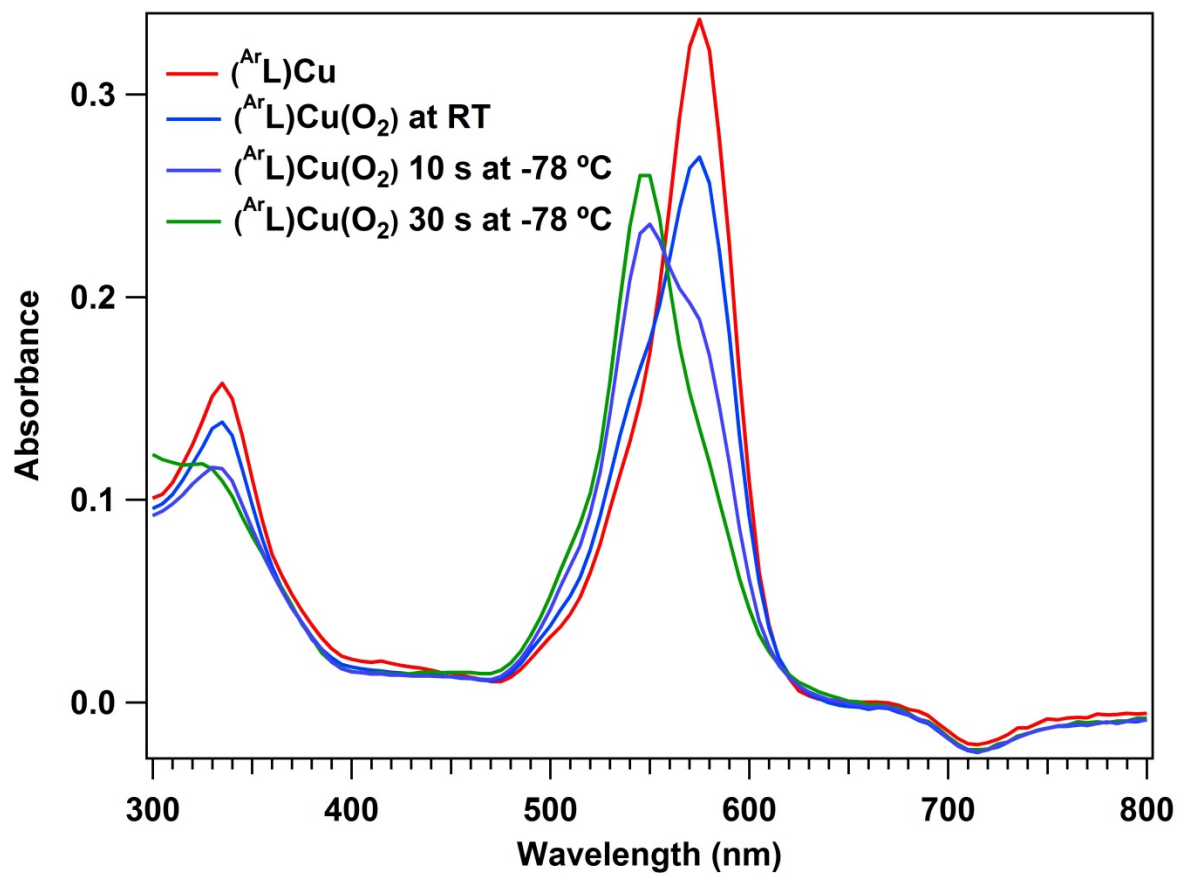


Figure S11. UV-Vis spectrum of $(^{Ar}L)Cu(O_2)$ reveals reversible O_2 binding to $(^{Ar}L)Cu$. Maximum absorption wavelengths for $(^{Ar}L)Cu$: 575 nm; $(^{Ar}L)Cu(O_2)$: 545 nm.

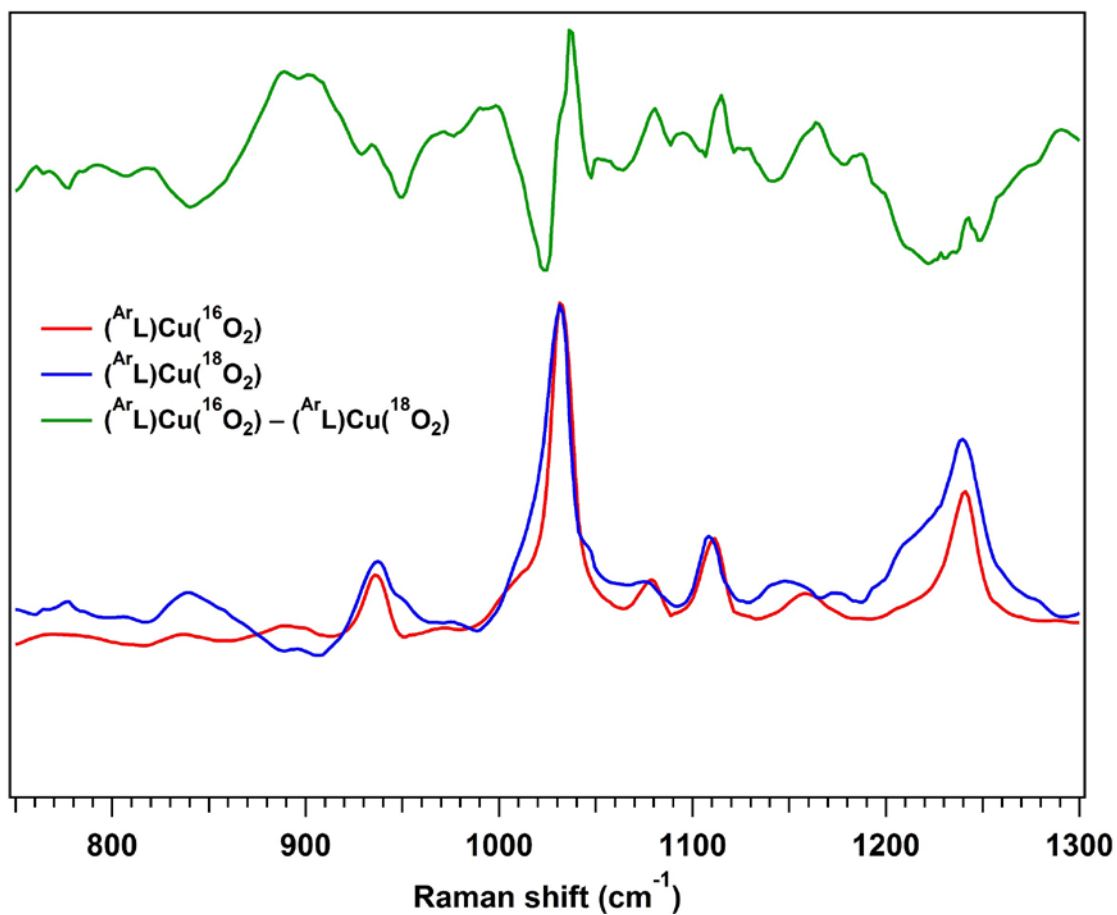


Figure S12. Raman spectra of $(^{Ar}L)Cu(O_2)$ on samples prepared with $^{16}O_2$ (red) and $^{18}O_2$ (blue); spectra were normalized relative to the band at 1030 cm^{-1} and a subtracted spectrum is shown on top in green. Spectra were collected in toluene, at room temperature, using $\lambda_{ex} = 532\text{ nm}$.

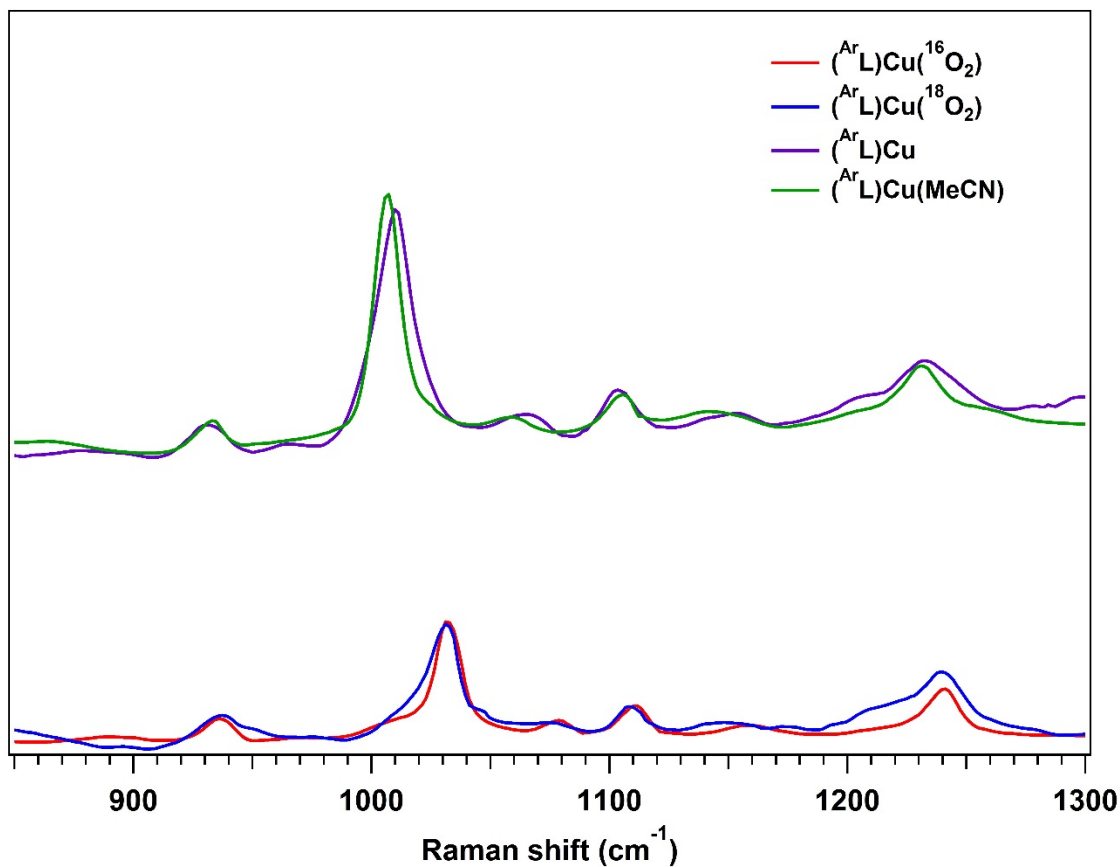


Figure S13. Raman spectra comparison for $(^{\text{Ar}}\text{L})\text{Cu}$ and $(^{\text{Ar}}\text{L})\text{Cu}(\text{O}_2)$: spectra for $(^{\text{Ar}}\text{L})\text{Cu}(\text{O}_2)$ samples prepared with $^{16}\text{O}_2$ (red) and $^{18}\text{O}_2$ (blue) normalized relative to the band at 1030 cm^{-1} ; spectra for $(^{\text{Ar}}\text{L})\text{Cu}$ (purple) and $(^{\text{Ar}}\text{L})\text{Cu}(\text{MeCN})$ (green), normalized relative to the band at 1010 cm^{-1} . Spectra were collected in toluene, at room temperature, using $\lambda_{\text{ex}} = 532\text{ nm}$. The data illustrate that the vibrations observed at 1010 cm^{-1} and 1030 cm^{-1} , respectively, are most likely ligand-related.

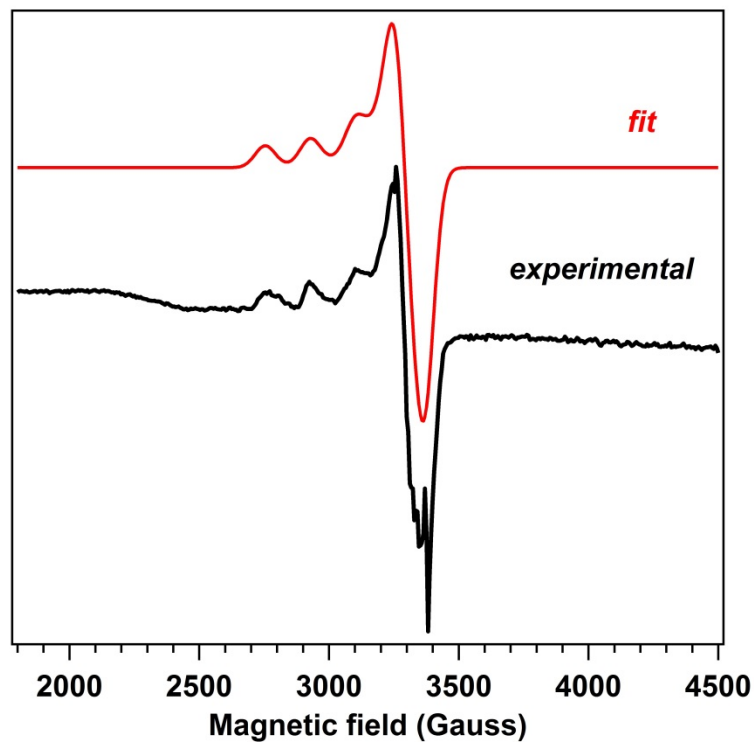


Figure S14. Frozen toluene EPR spectrum of complex **3** formed upon thermal decomposition of $(^{\text{Ar}}\text{L})\text{Cu}(\text{O}_2)$ expanded to show the rhombic signal (black), collected at 77 K, 9.453466 GHz. The red line represents a fit with Easyspin² for an $S = 1/2$ spin state, with the following parameters: $g_1 = 2.24$, $g_2 = 2.053$, $g_3 = 2.048$, $A_1 = 543$ MHz, $A_2 = 14.8$ MHz, $A_3 = 37.9$ MHz, linewidth = 7.80 mT.

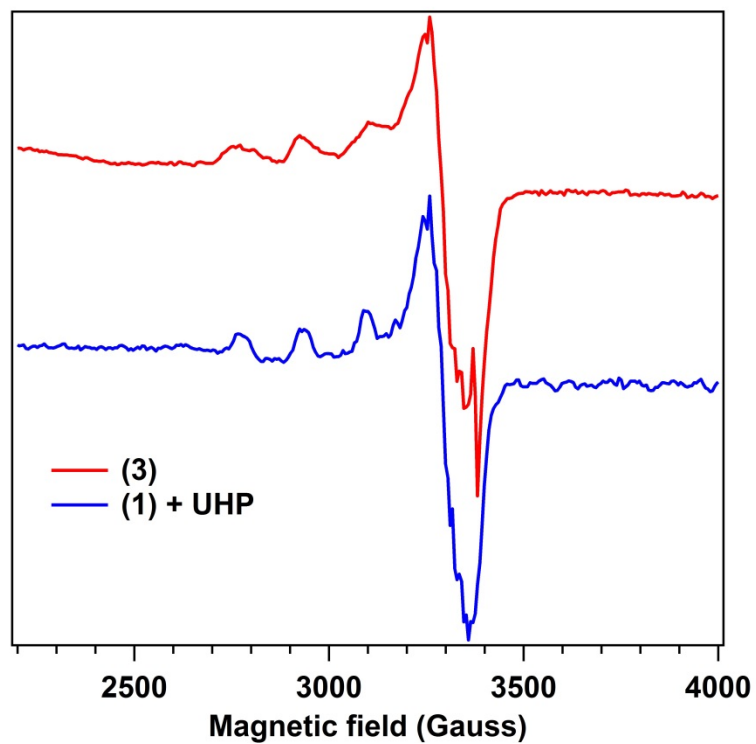


Figure S15. Frozen toluene EPR spectrum of the reaction mixture of (^{Ar}L)Cu and urea hydroperoxide at 65 °C (blue); EPR spectrum of product **3** (red). Spectrum was collected at 77 K, 9.449729 GHz.

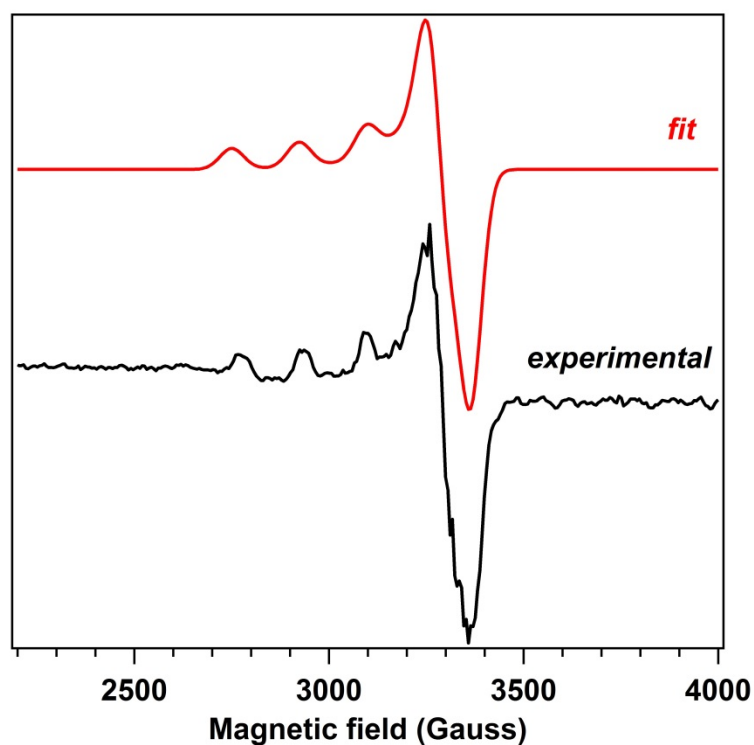


Figure S16. Fit for the frozen toluene EPR spectrum of the reaction mixture of (^AL)Cu and urea hydroperoxide at 65 °C (black). EPR spectrum was collected at 77 K, 9.449729 GHz. The red line represents a fit with Easyspin² for an $S = 1/2$ spin state, with the following parameters: $g_1 = 2.24$, $g_2 = 2.05$, $g_3 = 2.052$, $A_1 = 542$ MHz, $A_2 = 12.8$ MHz, $A_3 = 35.9$ MHz, linewidth = 6.11 mT.

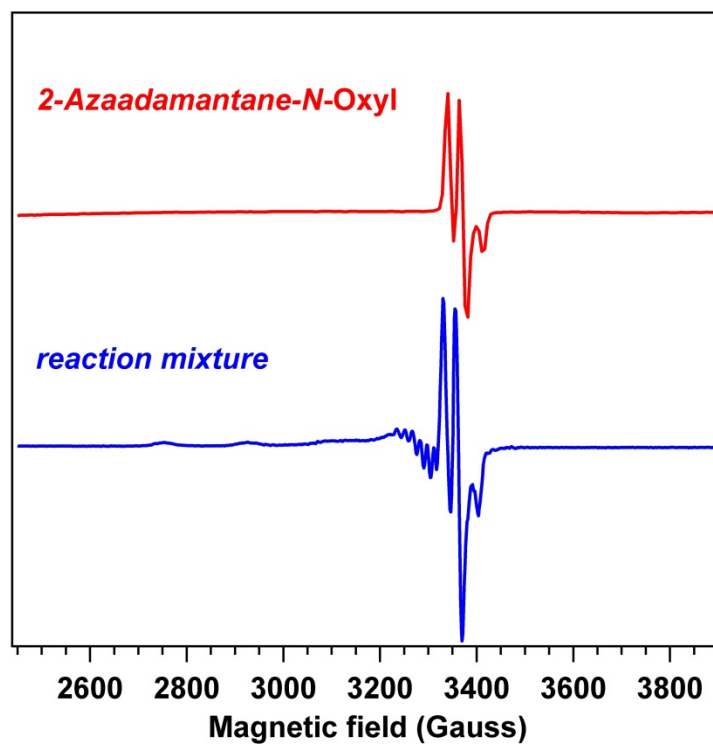


Figure S17. Frozen toluene EPR spectrum of the reaction mixture of (^{Ar}L)Cu(O₂) and 2-hydroxy-2-azaadamantane (blue); authentic 2-azaadamantane-*N*-oxyl EPR spectrum (red). Spectrum was collected at 77 K, 9.448212 GHz.

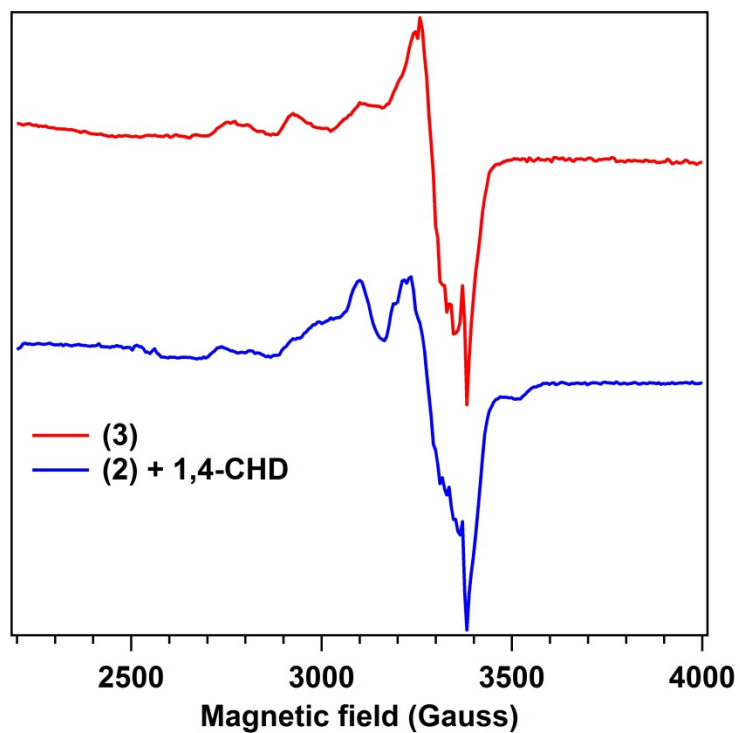


Figure S18. Frozen toluene EPR spectrum of the reaction mixture of (^{Ar}L)Cu(O₂) and 1,4-cyclohexadiene at 45 °C (blue); EPR spectrum of product **3** (red). Spectrum was collected at 77 K, 9.4462 GHz.

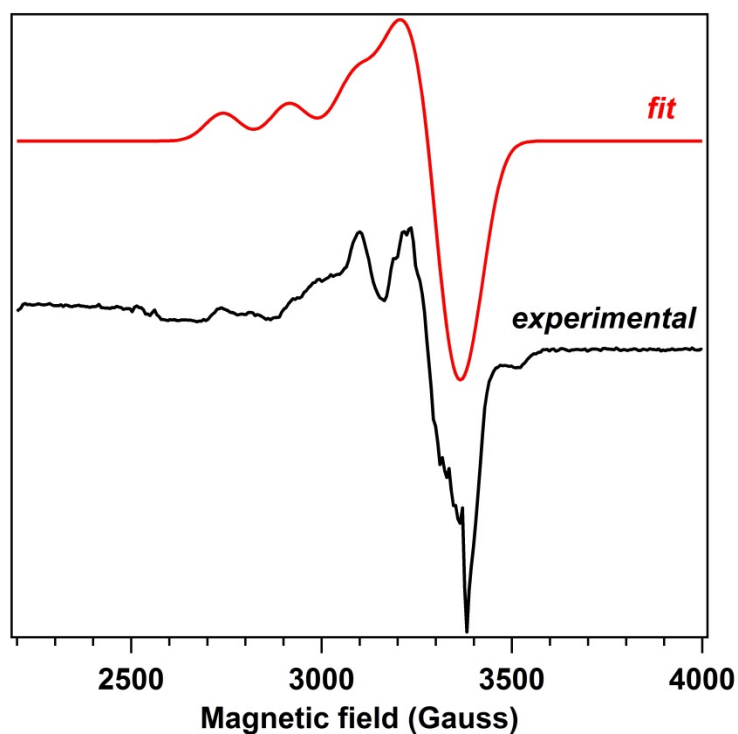


Figure S19. Fit for the frozen toluene EPR spectrum of the reaction mixture of (^ArL)Cu(O₂) and 1,4-cyclohexadiene at 45 °C (black). EPR spectrum was collected at 77 K, 9.4462 GHz. The red line represents a fit with Easyspin² for an $S = 1/2$ spin state, with the following parameters: $g_1 = 2.25$, $g_2 = 2.09$, $g_3 = 2.012$, $A_1 = 542$ MHz, $A_2 = 16.8$ MHz, $A_3 = 35.9$ MHz, linewidth = 9.0 mT.

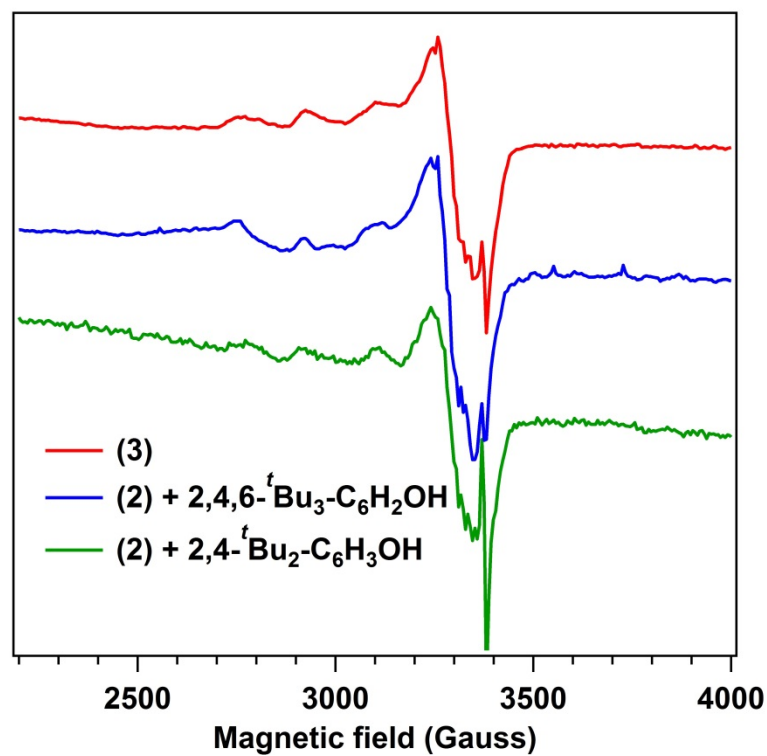


Figure S20. Frozen toluene EPR spectra of the reaction mixtures of (^{Ar}L)Cu(O₂) and phenols following HAA: (red) EPR spectrum of **3**; (blue) reaction with 2,4,6-tri-*tert*-butylphenol; (green) reaction with 2,4-di-*tert*-butylphenol. All spectra were collected at 77 K, 9.448072 and 9.451315 GHz, respectively.

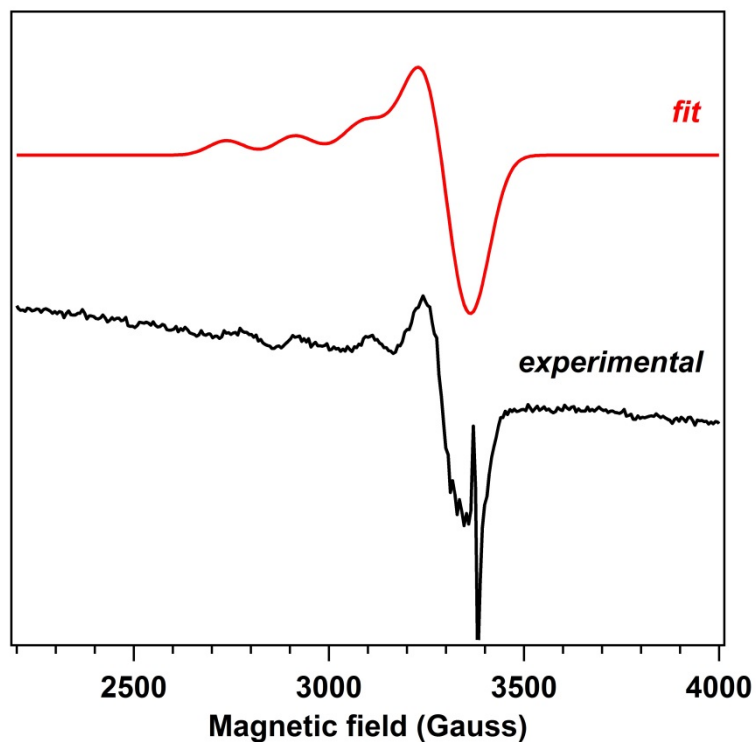


Figure S21. Fit for frozen toluene EPR spectrum of the reaction mixture of (^AL)Cu(O₂) and 2,4-di-*tert*-butylphenol (black); EPR spectrum was collected at 77 K, 9.451315 GHz. The red line represents a fit with Easyspin² for an $S = 1/2$ spin state, with the following parameters: $g_1 = 2.25$, $g_2 = 2.07$, $g_3 = 2.027$, $A_1 = 546$ MHz, $A_2 = 16.8$ MHz, $A_3 = 39.9$ MHz, linewidth = 9.0 mT.

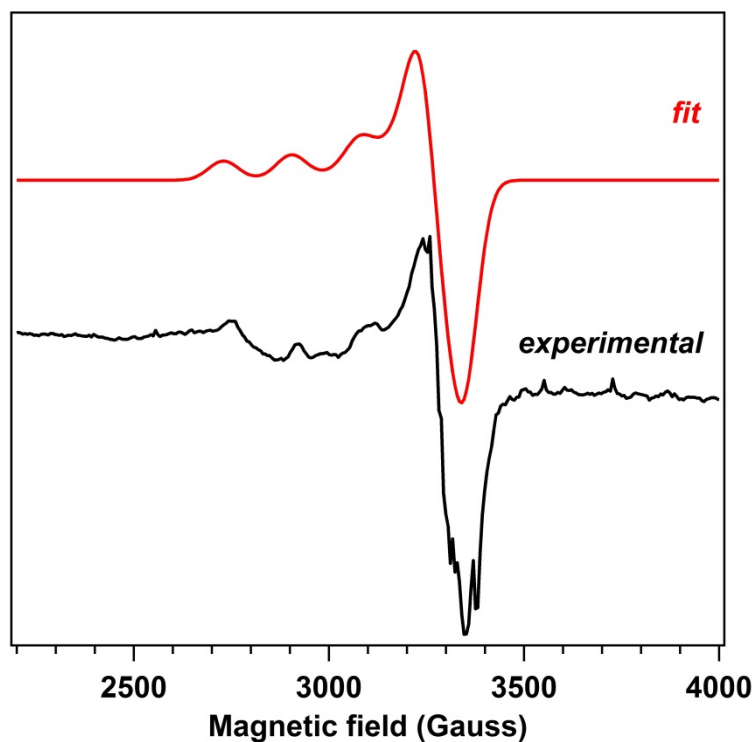


Figure S22. Fit for frozen toluene EPR spectrum of the reaction mixture of (A L)Cu(O₂) and 2,4,6-tri-*tert*-butylphenol (black); EPR spectrum was collected at 77 K, 9.448072 GHz. The red line represents a fit with Easyspin² for an $S = 1/2$ spin state, with the following parameters: $g_1 = 2.25$, $g_2 = 2.057$, $g_3 = 2.054$, $A_1 = 546$ MHz, $A_2 = 12.8$ MHz, $A_3 = 35.9$ MHz, linewidth = 7.59 mT.

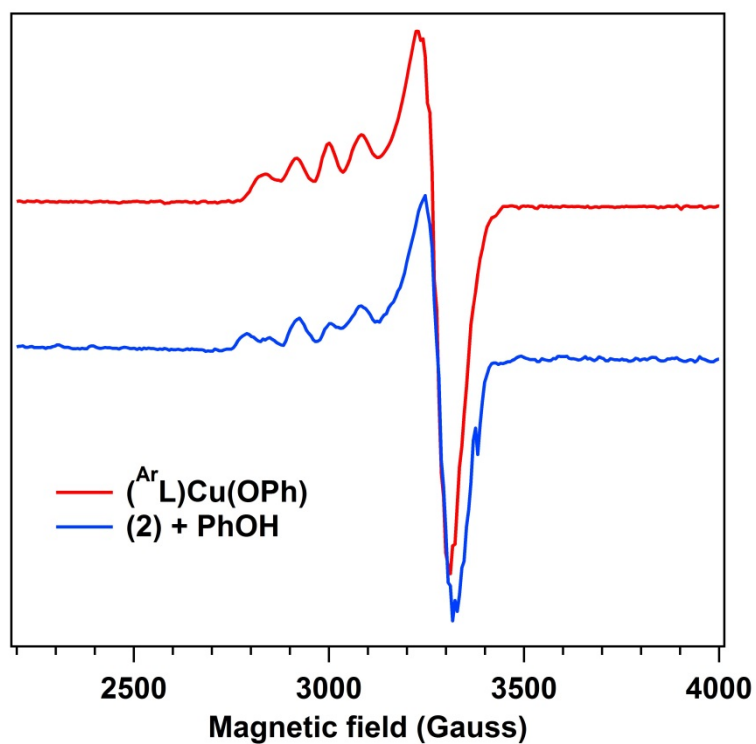


Figure S23. Frozen toluene EPR spectrum of the reaction mixture of $(^{Ar}L)Cu(O_2)$ and phenol (blue); EPR spectrum of authentic $(^{Ar}L)Cu(OPh)$ (7) (red). Spectrum was collected at 77 K, 9.451908 GHz.

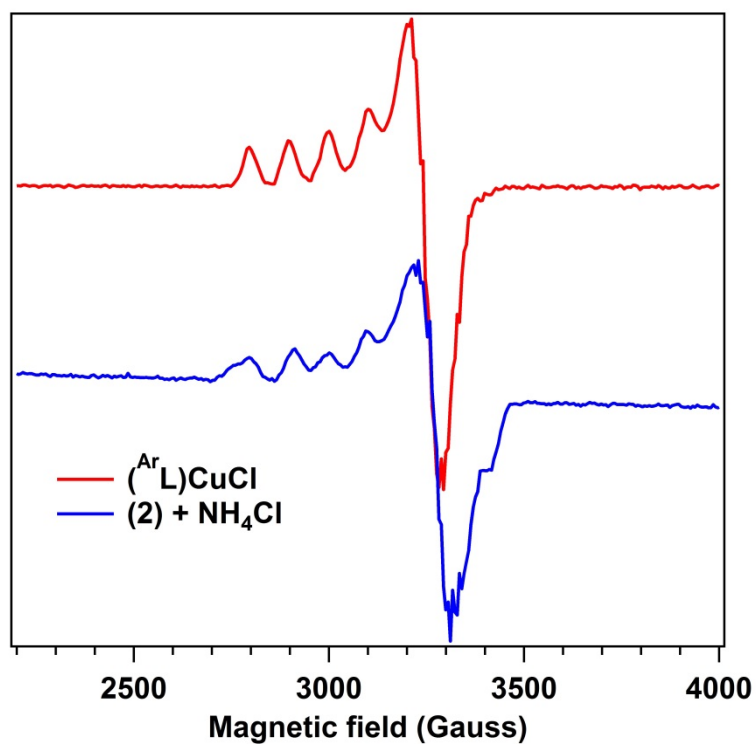


Figure S24. Frozen toluene EPR spectrum of the reaction mixture of $(^{\text{Ar}}\text{L})\text{Cu}(\text{O}_2)$ and ammonium chloride (blue); EPR spectrum of authentic $(^{\text{Ar}}\text{L})\text{Cu}(\text{Cl})$ (**5**) (red). Spectrum was collected at 77 K, 9.44302 GHz.

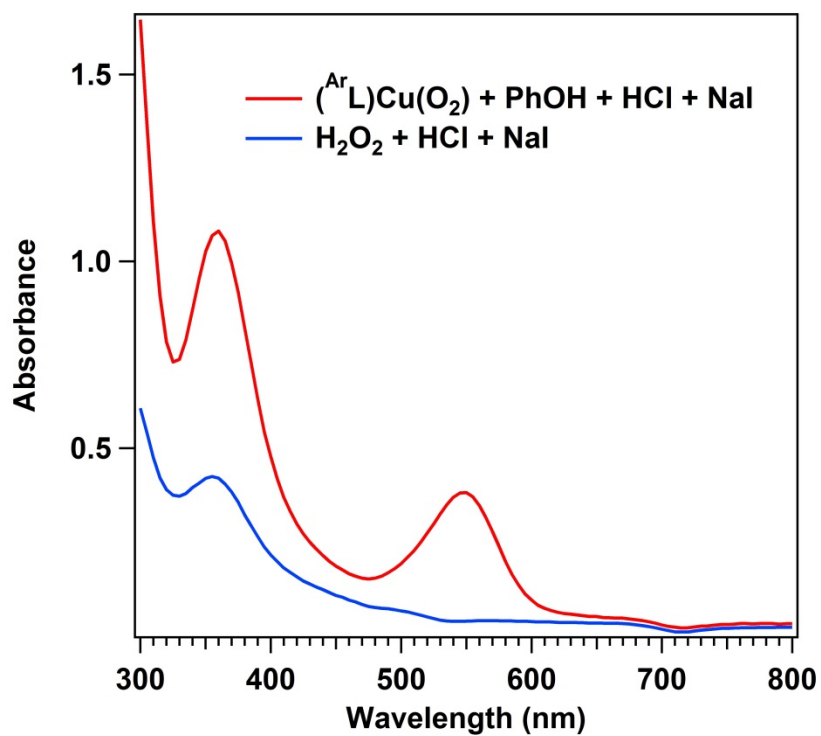


Figure S25. Iodometric detection of H_2O_2 formation via UV-Vis: spectrum of the reaction mixture of $(^{Ar}L)Cu(O_2)$ with phenol, quenched with HCl and treated with excess NaI in acetonitrile (red) ; spectrum for hydrogen peroxide treated with HCl and excess NaI in acetonitrile (blue); formation of I_3^- identified at 362 nm.

X-Ray Diffraction Techniques. All structures were collected on a Bruker three-circle platform goniometer equipped with an Apex II CCD and an Oxford cryostream cooling device. Radiation was from a graphite fine focus sealed tube Mo K α (0.71073 Å) source. Crystals were mounted on a cryoloop or glass fiber pin using Paratone N oil. Structures were collected at 100 K. Data was collected as a series of φ and/or ω scans. Data was integrated using SAINT⁴ and scaled with either a numerical or multi-scan absorption correction using SADABS⁴. The structures were solved by direct methods or Patterson maps using SHELXS-97⁵ and refined against F^2 on all data by full matrix least squares with SHELXL-97.⁵ All non-hydrogen atoms were refined anisotropically. Hydrogen atoms were placed at idealized positions and refined using a riding model. The isotropic displacement parameters of all hydrogen atoms were fixed to 1.2 times the atoms they are linked to (1.5 times for methyl groups). Further details on particular structures are noted below.

(^AL)Cu (1). The structure was solved in the triclinic space group $P\bar{1}$ with 2 molecules per unit cell.

(^AL)Cu(O₂) (2). The structure was solved in the triclinic space group $P\bar{1}$ with 2 molecules per unit cell.

(^AL)Cu(O-DMPO) (4). The structure was solved in the monoclinic space group $C2/c$ with 4 molecules per unit cell. One of the phenyl groups exhibited positional disorder and was refined using similarity constraints. The DMPO group exhibited positional disorder and was refined using similarity constraints, properly accounting for the symmetry of the molecule.

(^AL)CuCl (5). The structure was solved in the monoclinic space group $C2/c$ with 8 molecules per unit cell. A solvent mask was implemented in the Olex2 software to account for some minor hexanes solvent disorder.

(^AL)Cu(OEt) (6). The structure was solved in the monoclinic space group $P2_1/n$ with 4 molecules per unit cell. One of the aryl substituents exhibited positional disorder and was refined using similarity constraints. A solvent mask was implemented in the Olex2 software due to disordered hexanes and benzene solvent molecules present in the unit cell.

⁴ APEX2 Software Suite; Bruker AXS: Madison, WI, 2009.

⁵ Sheldrick, G. M. *Acta Crystallogr., Sect. A: Found. Crystallogr.* **2008**, 64, 112.

(^{Ar}L)Cu(OPh) (7). The structure was solved in the monoclinic space group $P2_1/n$ with 4 molecules per unit cell.

Table S1. X-ray diffraction experimental details^{a,b}

	(^{Ar} L)Cu (1)	(^{Ar} L)Cu(O ₂) (2)	(^{Ar} L)Cu(O-DMPO) (4)	(^{Ar} L)CuCl (5)	(^{Ar} L)Cu(OEt) (6)	(^{Ar} L)Cu(OPh) (7)
CCDC	1557369	1557370	1557371	1557372	1557373	1557374
Moiety Formula	C ₈₄ H ₆₇ CuN ₂ ; 3×(C ₆ H ₆)	C ₆₆ H ₄₉ CuN ₂ O ₂ ; 2×(C ₆ H ₆)	C ₇₂ H ₅₉ CuN ₃ O ₂	C ₆₆ H ₄₉ ClCuN ₂	C ₆₈ H ₅₄ CuN ₂ O	C ₇₂ H ₅₄ CuN ₂ O
FW	1167.95	1121.84	1061.77	969.07	978.68	1026.72
Crystal System	triclinic	triclinic	monoclinic	monoclinic	monoclinic	monoclinic
Space Group (Z)	<i>P</i> $\bar{1}$ (2)	<i>P</i> $\bar{1}$ (2)	<i>C</i> 2/ <i>c</i> (4)	<i>C</i> 2/ <i>c</i> (8)	<i>P</i> 2 ₁ / <i>n</i> (4)	<i>P</i> 2 ₁ / <i>n</i> (4)
a (Å)	12.446(4)	12.4948(7)	20.4795(12)	34.093(2)	19.6142(9)	19.3286(7)
b (Å)	14.203(4)	14.4326(8)	17.6321(10)	17.7142(12)	13.5161(6)	13.5791(8)
c (Å)	20.614(6)	18.0433(10)	15.3822(15)	23.3196(16)	20.0152(9)	20.9099(13)
α (°)	74.427(5)	96.006(1)	90	90	90	90
β (°)	84.895(5)	105.681(1)	97.214(4)	131.542(1)	96.137(2)	98.604(1)
γ (°)	64.576(5)	104.743(1)	90	90	90	90
Volume (Å³)	3168.6(16)	2976.5(3)	5510.5(7)	10514.0(12)	5275.8(4)	5426.4(5)
Calc. ρ (mg/m³)	1.224	1.252	1.280	1.221	1.232	1.257
μ (mm⁻¹)	0.393	0.418	0.952	0.507	0.460	0.451
Crystal Size (mm)	0.03×0.03×0.02	0.40×0.38×0.21	0.15×0.13×0.11	0.08×0.02×0.02	0.26×0.18×0.13	0.11×0.11×0.06
Reflections	12132	10615	4751	10363	9231	9626
Completeness (to 2θ)	99.2%	100%	97.2%	100%	98%	97.4%
	25.82°	25.112°	66.769°	25.997°	24.940°	25.067°
GOF on F²	1.006	1.029	1.036	0.999	1.058	1.048
R1, wR2^c [I>2σ(I)]	0.058, 0.1482	0.0322, 0.0781	0.0501, 0.1561	0.0477, 0.1036	0.0691, 0.1388	0.0647, 0.1413

^a λ = 0.71073 Å; ^b T = 100(2) K; ^c R1 = Σ||F_o|-|F_c||/Σ|F_o|, wR2 = {Σ[w(F_o²-F_c²)²]/Σ[w(F_o²)²]}^{1/2}

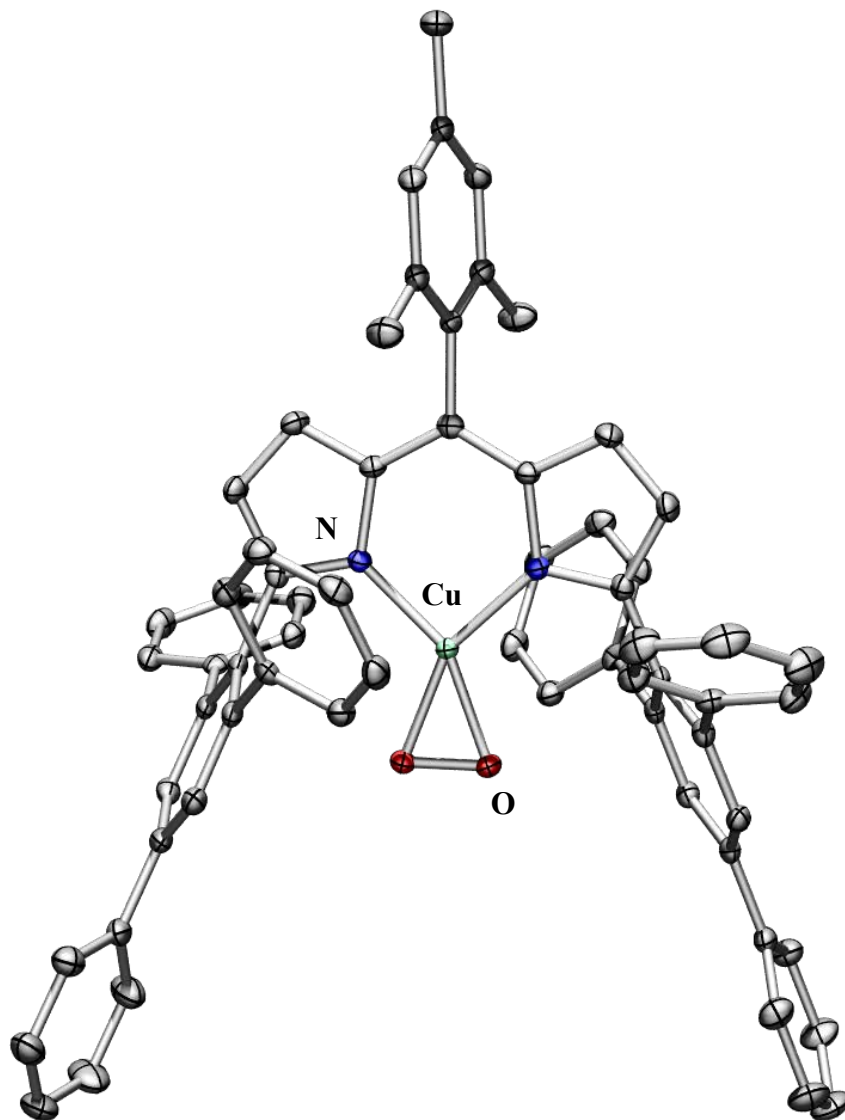


Figure S27. Solid-state molecular structure for $(^{\text{ArL}}\text{Cu}(\text{O}_2))$ (2) with thermal ellipsoids at 50% probability level. Hydrogens and benzene solvent in the unit cell omitted for clarity.

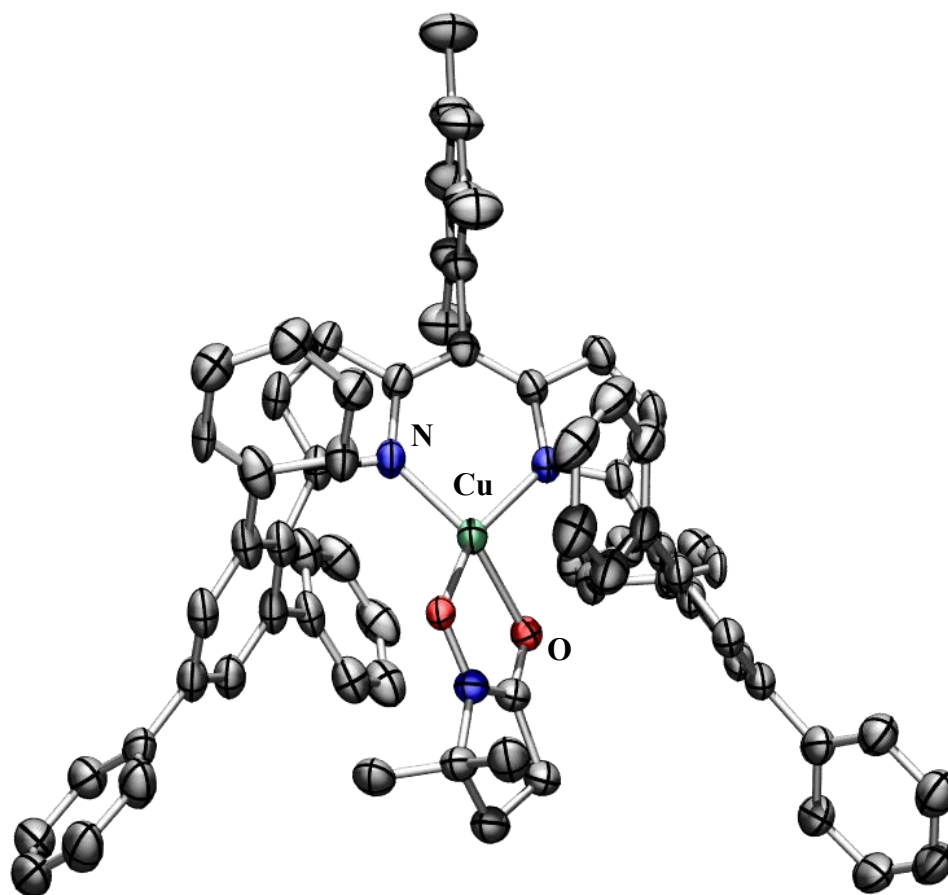


Figure S28. Solid-state molecular structure for $(^{Ar}L)Cu(O-DMPO)$ (**4**) with thermal ellipsoids at 50% probability level. Hydrogens, disordered phenyl and DMPO units omitted for clarity

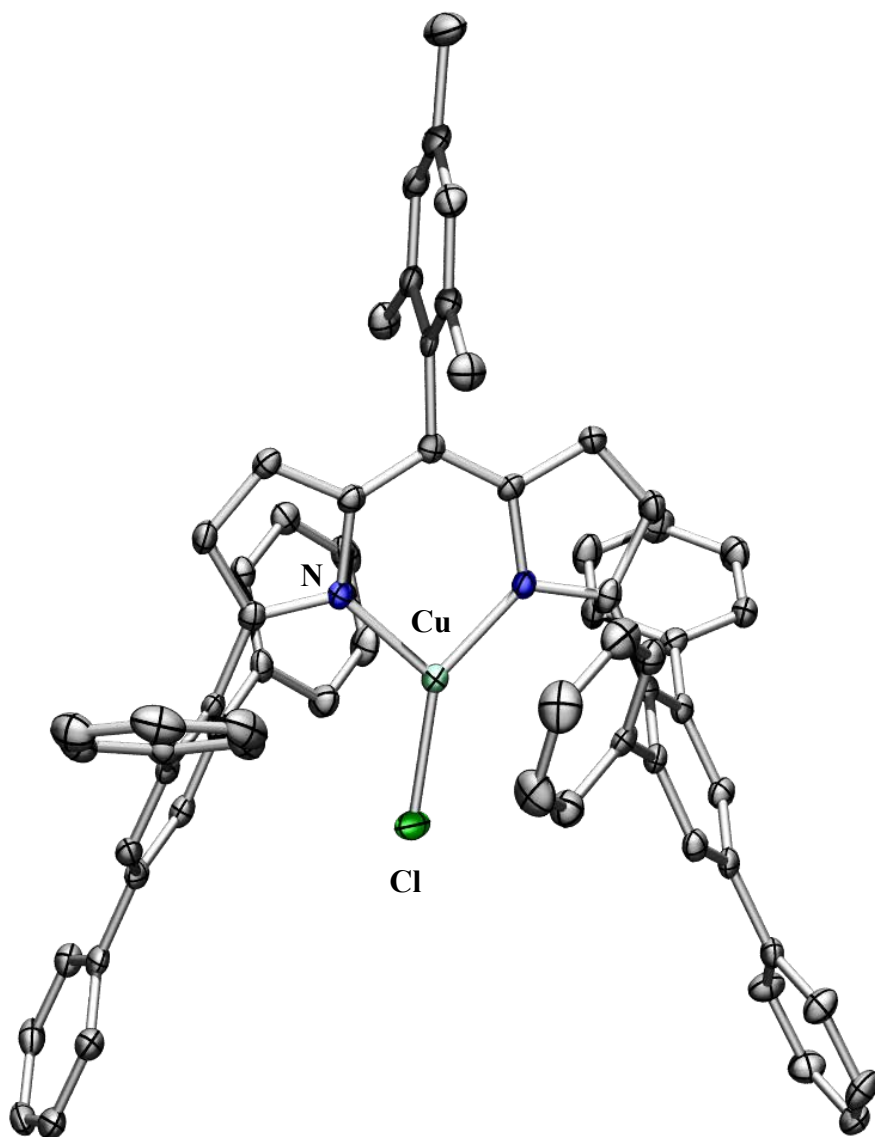


Figure S29. Solid-state molecular structure for $(^A L)CuCl$ (**5**) with thermal ellipsoids at 50% probability level. Hydrogens and benzene solvent in the unit cell omitted for clarity.

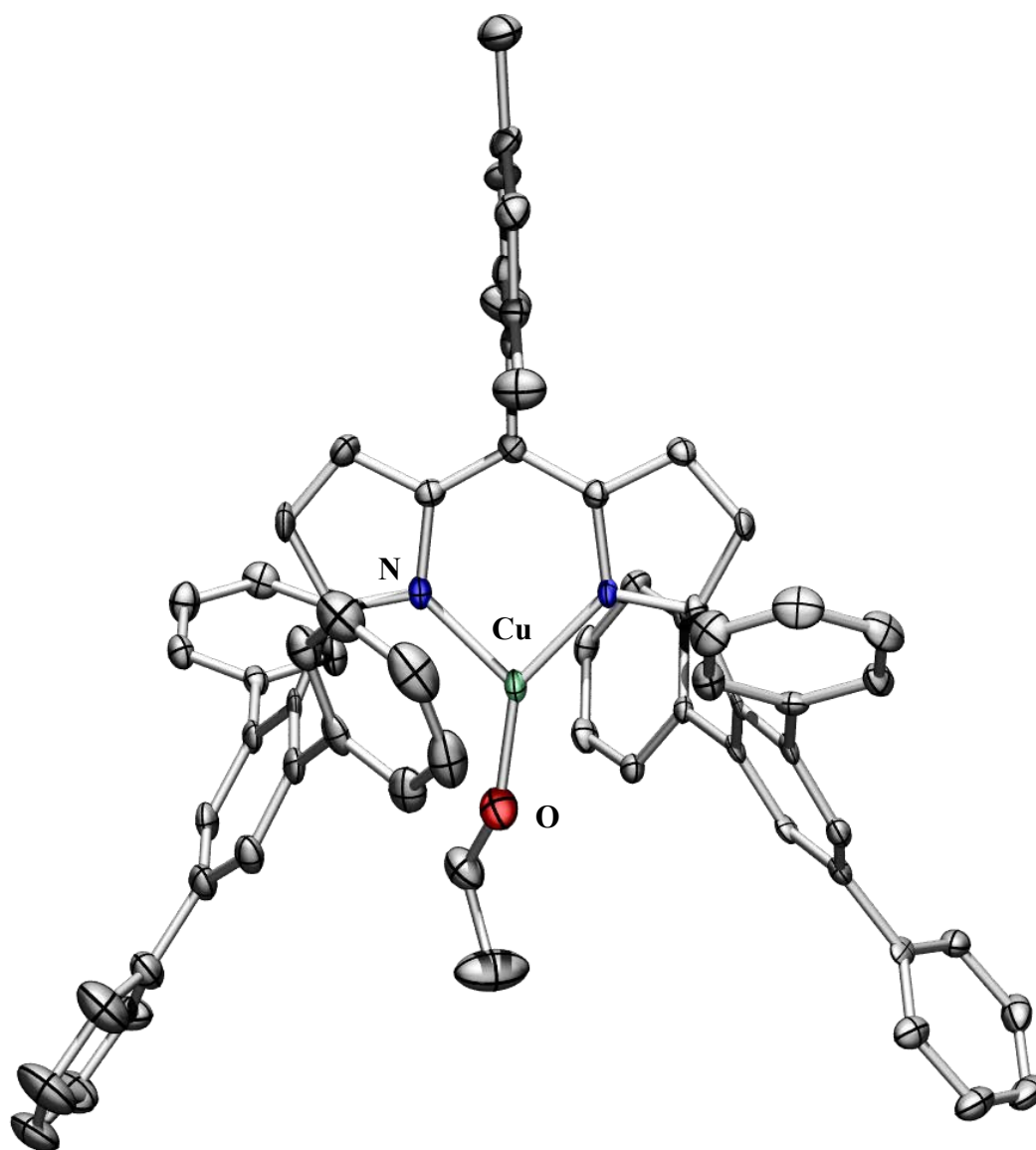


Figure S30. Solid-state molecular structure for $(^{\text{ArL}}\text{Cu}(\text{OEt}))$ (**6**) with thermal ellipsoids at 50% probability level. Hydrogens and benzene solvent in the unit cell omitted for clarity.

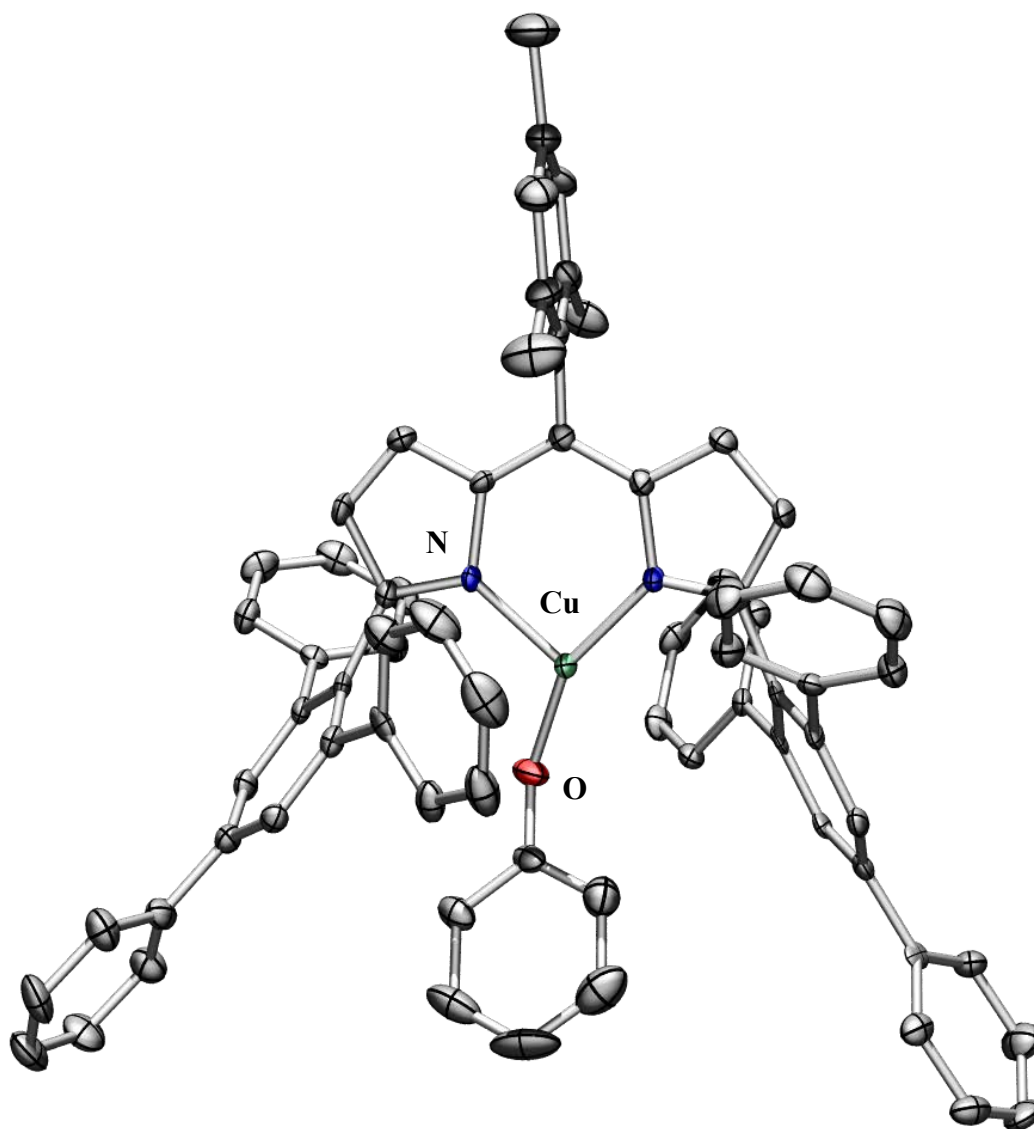


Figure S31. Solid-state molecular structure for $(^{\text{Ar}}\text{L})\text{Cu}(\text{OPh})$ (7) with thermal ellipsoids at 50% probability level. Hydrogens and benzene solvent in the unit cell omitted for clarity.

Computational Methods. Computations were carried out utilizing the ORCA 3.0.3⁶ program package. The B3LYP⁷ functional was used with the def2-TZVP (Cu, N, Cl) and def2-SV(P) (C, H) basis sets⁸. For single point calculations and property calculations the def2-TZVP/J (Cu, N, Cl) and def2-SVP/J (C, H) auxiliary basis sets⁹ were employed to utilize the RIJCOSX¹⁰ approximation for accelerating the calculation. A broken symmetry approach as previously described¹¹ was attempted, however, no such $S = 0$ solution resulting from a Cu^{II} antiferromagnetically coupled to a superoxide anion was identified.

CASSCF Solution. A complete active space self-consistent field (CASSCF) approach as presented previously¹² for analogous copper dioxygen complexes was employed instead. To minimize computational time, the ligand was truncated converting the 2,4,6-Ph₃-C₆H₂ into a simple phenyl unit (^{Ph}L)Cu(O₂) (**2'**). A CAS(2,2) reference space (CAS(m,n) refers to the active space comprising m electrons in n orbitals) was found to be sufficient to describe the representative active space, in line with calculations reported for a similar β -diketiminato copper dioxygen complex.^{12,13} This active space describes the bonding and antibonding combination of the interaction between d_{xz} and $\pi^*_{O_2}$ orbitals. A CAS(4,3) calculation was also undergone, incorporating the orthogonal $\pi^*_{O_2}$ orbital, however, an occupation of 1.999997 was identified for the additional orbital, with little invariance for the other two orbitals considered above.

The two active orbitals 131 and 132 (from CAS(2,2)) were found to possess occupations of 1.653589 and 0.346411, respectively (Fig. S8a). The final energy was found $E = -3047.2672302896 E_h$. The contributions of the singlet ground state and singlet excited state determined are illustrated in Table S2.

⁶ Neese, F. *WIREs Comput. Mol. Sci.* **2012**, 2, 73.

⁷ (a) Becke, A. D. *J. Chem. Phys.* **1993**, 98, 5648; (b) Lee, C. T.; Yang, W. T.; Parr, R. G. *Phys Rev. B* **1988**, 33, 785.

⁸ (a) Schäfer, A.; Horn, H.; Ahlrichs, R. *J. Chem. Phys.* **1992**, 97, 2571; (b) Schäfer, A.; Huber, C.; Ahlrichs, R. *J. Chem. Phys.* **1994**, 100, 5829; (c) Weigend, F.; Ahlrichs, R. *Phys. Chem. Chem. Phys.* **2005**, 7, 3297.

⁹ Weigand, F. *Phys. Chem. Chem. Phys.* **2006**, 8, 1057.

¹⁰ Neese, F.; Wennmohs, F.; Hansen, A.; Becker, U. *Chem. Phys.* **2009**, 356, 98.

¹¹ Kirchner, B.; Wennmohs, F.; Ye, S.; Neese, F. *Curr. Opin. Chem. Biol.* **2007**, 11, 134.

¹² Tomson, N. C.; Williams, K. D.; Dai, X.; Sproules, S.; DeBeer, S.; Warren, T. H.; Wieghardt, K. *Chem. Sci.* **2015**, 6, 2474.

¹³ (a) Gherman, B.; Cramer, C. *Inorg. Chem.* **2004**, 43, 7281; (b) Zapata-Rivera, J.; Caballol, R.; Calzado, C. J. *J. Comput. Chem.* **2011**, 32, 1144; (c) Zapata-Rivera, J.; Caballol, R.; Calzado, C. J. *Phys. Chem. Chem. Phys.* **2011**, 13, 20241; (d) Cramer, C. J.; Gour, J. R.; Kinal, A.; Włoch, M.; Piecuch, P.; Shahi, A. R. M.; Gagliardi, L. *J. Phys. Chem. A* **2008**, 112, 3754.

Table S2. Percent contributions of the two singlet configurations to the ground state wavefunctions.

Percent contribution (%)	Representative electron configurations	
	131	132
82.68	2	0
17.32	0	2

Further localization of these orbitals in ORCA⁶ (Fig. S8b) allowed for identification of valence bond contributions from the three possible configurations to the ground state (Table S3). Energy found $E = -3047.267230102 E_h$.

Table S3. Valence bond analysis of CAS(2,2) wavefunctions.

Configuration weight	Representative electron configurations		Valence bond description
	131	132	
0.87120	1	1	Cu ^{II} /O ₂ ^{•-}
0.09403	2	0	Cu ^I /O ₂ ⁰
0.03477	0	2	Cu ^{III} /O ₂ ²⁻

Table S4. XYZ Coordinates for (^{Ph}L)Cu(O₂) (**2'**) used for the CASSCF calculation.

Cu 4.049000 3.120000 4.142000
O 5.591000 3.960000 3.606000
O 5.380000 4.067000 4.968000
N 2.763000 2.636000 5.421000
N 3.241000 2.290000 2.661000
C 2.002000 1.653000 2.699000
C 3.675000 2.266000 1.382000
C 1.682000 1.784000 5.163000
C 4.510000 3.571000 8.400000
C 4.447000 6.198000 7.485000
C 5.344000 3.748000 0.176000
C 0.032000 0.580000 3.741000
C 5.331000 5.866000 8.514000
C 1.668000 1.266000 1.381000
C 7.732000 3.279000 0.368000

C 3.589000 5.261000 6.915000
C 2.700000 1.653000 0.559000
C 2.738000 2.916000 6.741000
C 1.299000 1.379000 3.878000
C 5.342000 4.547000 8.966000
C -1.206000 1.238000 3.691000
C 5.059000 2.658000 1.024000
C 0.104000 -0.815000 3.621000
C -2.356000 0.476000 3.495000
C 7.428000 2.219000 1.226000
C 1.019000 1.527000 6.389000
C 3.634000 3.926000 7.359000
C -2.312000 -0.903000 3.324000
C 6.121000 1.895000 1.554000
C 1.682000 2.225000 7.366000
C -1.074000 -1.532000 3.398000
C 6.675000 4.026000 -0.146000
C 1.425000 -1.536000 3.732000
C -3.575000 -1.691000 3.075000
C -1.318000 2.736000 3.833000
H -0.473000 3.202000 3.371000
H -2.216000 3.073000 3.358000
H -1.344000 2.995000 4.871000
H 2.160000 -0.874000 4.140000
H 1.315000 -2.386000 4.373000
H 1.737000 -1.860000 2.761000
H -1.022000 -2.594000 3.281000
H -3.305000 0.969000 3.475000
H -3.395000 -2.726000 3.277000
H -4.352000 -1.332000 3.717000
H -3.873000 -1.573000 2.054000
H 2.756000 1.517000 -0.501000
H 0.774000 0.763000 1.078000
H 0.160000 0.904000 6.527000
H 1.442000 2.241000 8.409000
H 6.889000 4.839000 -0.808000
H 8.227000 1.641000 1.642000
H 6.001000 4.273000 9.763000
H 4.428000 7.205000 7.123000
H 8.745000 3.510000 0.114000
H 4.553000 4.353000 -0.215000
H 5.918000 1.071000 2.206000
H 5.980000 6.601000 8.942000
H 4.541000 2.563000 8.758000
H 2.903000 5.553000 6.148000